Evaluation and improvement of Gay-Berne interaction potential to simulate 3D DLVO interaction of clay particles

Angela Casarella[1*], Alessandro Tarantino[2], Vincent Richefeu[1], Alice di Donna[1]

[1] Univ. Grenoble Alpes, CNRS, Grenoble INP, 3SR, 38000, Grenoble (France)

[2] University of Strathclyde, Department of Civil and Environmental Engineering, G1 1XJ, Glasgow, Scotland (UK)

* Corresponding author: angela.casarella@3sr-grenoble.fr

ABSTRACT

This paper first presents a set of DLVO-based energy-separation functions for a pair of finite uniformly charged square platelets of infinitesimal thickness in three elementary configurations: face-to-face, edge-to-edge, and edge-to-face. The novel dataset was generated by summing the electrostatic interaction energy computed numerically by solving the non-linear 3D Poisson-Boltzmann equation and the van der Waals interaction energy calculated analytically. The dataset aims to inform qualitatively and quantitatively the energy/force separation functions used in the Discrete Element Method (DEM) and Coarse-Grained Molecular Dynamics (CGMD) modelling of clays. The same dataset was then used to calibrate and evaluate two Gay-Berne (GB)-type potentials: i) a DLVO-adapted Gay-Berne potential, where the Born-van der Waals branches of the underlying Lennard-Jones (LJ) potential are replaced with van der Waals-Columbic branches to represent DLVO interactions; ii) the Mie potential, where the exponents of the two energy terms are 'unlocked' instead of being set equal to 12 and 6 as per the original LJ potential. It is shown that the orientation parameter, μ, and the anisotropy parameter, ν, need to be different from μ=2 and ν=1 as adopted in CGMD clay modelling to capture the progression of the shape of the pair energy-separation function from face-to-face to edge-to-face and

This is a peer-reviewed, version of record of the following paper: Casarella, A., Tarantino, A., Richefeu, V., & Di Donna, A. (in press). Evaluation and improvement of Gay-Berne interaction potential to simulate 3D DLVO interaction of clay particles. Computers and Geotechnics.

edge-to-edge configuration. It is also shown that the MIE potential (with exponents m=3 and n=1.5) better captures the slow decay of the electrostatic repulsive energy component of the DLVO potential energy Coulombic branch of the interaction potential compared to the DLVO-adapted GB potential, which embeds the Lennard-Jones (LJ) exponents m=12 and n=6.

Keywords:
Gay-Berne potential, DLVO, Coulombic forces, van der Waals forces, clay, energy-separation function

1 INTRODUCTION

Particle-scale clay models are powerful tools to elucidate the mechanical processes occurring at the macroscale and inform continuum-scale constitutive models. Fully Atomistic Molecular Dynamics (FAMD) has been used to model the interaction of a pair of clay particles starting from interatomic potentials. However, a FAMD simulation of a cluster of clay particles would require computing millions of interactions between the digital representation of each atom and molecule in the clay-water system. Coarse-Grained Molecular Dynamics (CGMD) models are a valuable alternative to reduce the computational cost of the simulations as they simplify the molecular description of the system by reducing the number of degrees of freedom.

In CGMD simulations, individual atoms coalesce into fewer coarse-grained sites. A single clay particle can be modelled with i) a multi-site approach, where the coarse-grained sites are 'bonding' spheres (Anderson and Lu, 2001; Liu et al., 2015; Sjoblom, 2016; Jaradat and Abdelaziz, 2019; Pagano et al., 2020; de Bono and McDowell 2022) or ii) an individual platelet approach, where clay particles are modelled using cuboidal, ellipsoidal, or discoidal elements (Yao and Anandarajah, 2003; Ebrahimi et al. 2016; Kang et al. 2020; Sun et al. 2020; Bandera et al. 2021).

Particle-scale simulation tools where clay particles are modelled as single elements can be highly computationally efficient. However, they require the definition of a force-separation or energy-separation function. Existing approaches to model clay with 3D discrete simulations usually employ the Gay-Berne (GB) potential (Gay and Berne, 1981) to describe the interaction potential energy between clay particles (Plimpton, 1995; Thompson et al., 2022). The GB potential allows for simulations of three-dimensional systems of ellipsoids of various aspect ratios interacting at different orientations and separation distances and is characterised by 4 degrees of freedom. However, the GB model parameters do not have a clear physical meaning and must be calibrated against known interaction energy for a pair of particles (Bandera et al. 2021).

Two main calibration approaches can be found in the literature. Ebrahimi et al. (2014) and Honório et al. (2018) fitted the separation-energy relationship for oblate ellipsoids in face-to-face and edge-to-edge

configuration based on FAMD simulations of 'single-layer' kaolin clay particles with aspect ratio 1:5 combined with experimental data obtained from Atomistic Force Measurements (AFM). However, this approach is limited by the over-simplistic assumptions about particle geometry, which is somehow inevitable owing to the high computational cost of the FAMD simulations. Bandera et al. (2021) fitted the energy-separation function based on the DLVO closed-form solution derived for infinitely extended-infinitely thick-uniformly charged parallel particles (Derjaguin and Landau, 1941; Verwey and Overbeek, 1948). Yet, the assumption of infinite plates ignores the interaction forces arising at the platelet ends, which play a crucial role when clay particles are arranged in an edge-to-face configuration.

The DLVO theory provides a convenient calibration framework, embedding the combined effect of pore-fluid temperature, dielectric permittivity, and electrolyte concentration. For a rigorous calibration based on the DLVO theory, it is essential to conduct a 3D analysis of the particle-to-particle interaction considering their finite size and possibly including configurations different from elementary ones generally used to calibrate the GB potential (face-to-face, edge-to-edge).

The study presented in this paper aims to develop a DLVO-consistent energy interaction function that accounts for the finite size of particles, is calibrated against energy-separation functions for elementary configurations, and is validated against a generic particle-pair configuration. The paper first investigates the energy-separation function for elementary particle configurations (face-to-face, edge-to-face, edge-to-edge) based on the DLVO theory. The energy-separation function is derived for rigid, square, uniformly charged and infinitesimally thick particles as the sum of the electrostatic Coulombic energy and the van der Waals pair energy. The electrostatic component is computed numerically by solving the non-linear 3D Poisson-Boltzmann (PB) equation with the Finite Element (FE) method using the FE code COMSOL Multiphysics ® v. 6.1. The van der Waals component is computed analytically by integrating the fundamental molecule-to-molecule interaction over two flat plates at any given relative orientation. The numerical derivation of the DLVO interaction energy is verified against the analytical DLVO formulation for infinitely extended-infinitesimal thickness plates and low surface electrical potential/charge.

The 3D DLVO-based interaction is employed to i) calibrate the GB model parameters against elementary configurations and ii) assess the performance of the GB model for a generic 3D particle configuration by benchmarking the GB simulation against the provided DLVO solution. This allows revisiting the current GB formulations and proposing a generalised GB formulation (based on Mie potential, Mie (1903)) to accurately describe the interaction of finite clay particles at arbitrary relative orientation and model the constitutive interaction function. The generalised GB model proposed in this paper will be critical to developing robust Discrete Element Method (DEM) and Coarse-Grained Molecular Dynamics (CGMD) models.

2 DLVO THEORY

The DLVO theory assumes that the interaction between two charged particles in an electrolyte solution depends on the balance of electrostatic Coulombic forces and van der Waals attractive forces acting between the particles (Derjaguin, 1940; Verwey and Overbeek, 1948).

Coulombic forces result from the interaction between electric double layers (EDLs). When a charged object is immersed in a polar fluid, it attracts ions of opposite charge and repels ions of like charge. This results in an excess of ions of one sign at the particle surface (screening phenomenon, Debye and Hückel (1923)). Hence, a single charged clay particle in a polar fluid is surrounded by an EDL. The first layer of the EDL is formed by the charged ions firmly attached to the particle surface (Stern layer). The second layer consists of a non-uniform distribution of ions electrically attracted by the particle surface charge and subjected to a progressive thermal motion that drives them away from the particle itself. As a result, the electrostatic potential decays exponentially with the distance from the particle charged surface.

At particle distances from 10 nm down to interatomic spacing (about 0.2 nm), weak attractive van der Waals forces originate from the correlations in the fluctuating polarisations of nearby particles (Israelachvili, 2011).

2.1 Electrical Double Layer

Within the DLVO framework, the electrostatic energy, U_{Edl}, can be computed from the electrical potential field, $\phi(x,y,z)$ [V], in turn, derived from the Poisson-Boltzmann (PB) equation:

$$\nabla^2\phi(x,y,z) = \frac{\delta^2\phi}{\delta x^2} + \frac{\delta^2\phi}{\delta y^2} + \frac{\delta^2\phi}{\delta z^2} = -\frac{c_0 e}{\varepsilon}\left(exp\left(-\frac{v_i e\phi(x,y,z)}{kT}\right) - exp\left(\frac{v_i e\phi(x,y,z)}{kT}\right)\right) \quad [1]$$

where c_0 [ion/m^3] is the reference concentration taken at a considerable distance from the surface, e is the charge of the electron [e=1.602E−19 C], v_i is the valence, k is the Boltzmann constant [k=1.38E−23 J K^{-1}], T [K] is the absolute temperature, and ε [C^{2}J^{-1}m^{-1}] is the dielectric permittivity equal to the product of the dielectric permittivity in vacuum, ε_0 [ε_0=8.8542E−12 C^{2}J^{-1}m^{-1}], and the relative dielectric permittivity, ε_r [-].

The PB equation is highly non-linear and is solved numerically in this work. While there is no controversy about using the PB equation to determine the electric potential field distribution around a clay particle, deriving the free energy of interacting EDLs is not straightforward. Several approaches have been proposed for the electrostatic free energy of colloidal systems. Within the framework of classical thermodynamics (Verwey and Overbeek, 1948; Derjaguin, 1940), the interaction energy is associated with the 'free' energy. Once computed the electric potential distribution, ϕ(x,y,z), one can calculate U_{Edl} knowing that the thermodynamically preferred structure of an EDL is the one that minimises the variation of free energy of the system (Gray and Stiles, 2018). However, choosing the most appropriate free energy (Gibbs, Helmholtz, Grand Potential, or others) is not straightforward.

According to the recent work by Gupta et al. (2020), when two charged plates are immersed in an extensive electrolyte reservoir, it is convenient to minimise the Grand Potential Ω [J]. In statistical mechanics, the Grand Potential is a quantity used to define the free energy of a system defined as $\Omega \equiv U - TS - \mu N$, where U is the internal energy, T is the temperature of the system, S is the entropy, μ is the chemical potential, and N is the number of particles in the system. Assuming Ω_0 [J] as the Grand Potential of the large reservoir of electrolyte in which the considered charged surfaces are immersed, one can compute the variation of Grand Potential (Gupta et al., 2020) as:

$$\Omega - \Omega_0 = -\int_V \left(\frac{\varepsilon}{2}|\nabla\phi|^2 + kT\sum_i (c_i - c_0)\right)dV + \int_B \sum_j q_j\phi_j dB - U_{charge} \quad [2]$$

where V [m^3] is the system volume, B [m^2] represents all the boundaries indexed by j, ϕ_j [V] and q_j [C/m^2] are the electric potential and the charge density respectively at the jth surface, c_i [ion/m^3] is the concentration of the ith ion type, c_0 [ion/m^3] is the reference ions concentration taken at a considerable distance from the particle surfaces, and U_{charge} [J] is the energy required to charge the surfaces. U_{charge} needs to be appropriately modified to account for different boundary conditions. By definition, under constant surface charge conditions, no energy is required to charge the considered surfaces; thus, U_{charge}=0. In contrast, when the boundaries are maintained at constant surface potential, $U_{charge}\neq 0$, and Gupta et al. (2020) propose:

$$U_{\text{charge}} = \int_B \sum_j q_j\phi_j d^2\boldsymbol{r_j} \quad [3]$$

As a result, the variation of grand potential for planar surfaces at constant surface potential can be computed as:

$$\Omega - \Omega_0 = -\int_V \left(\frac{\varepsilon}{2}|\nabla\phi|^2 + kT\sum_i (c_i - c_0)\right)dV \quad [4]$$

On the other hand, for planar surfaces at constant charge (U_{charge}=0):

$$\Omega - \Omega_0 = -\int_V \left(\frac{\varepsilon}{2}|\nabla\phi|^2 + kT\sum_i (c_i - c_0)\right)dV + \int_B \sum_j q_j\phi_j dB \quad [5]$$

The free energy of the interacting electrical double layers, U_{Edl}, is calculated by assuming that the free energy is equal to zero when the separation distance between the particles goes to infinity:

$$U_{\text{Edl}} = (\Omega - \Omega_0) - (\Omega - \Omega_0)_\infty \quad [6]$$

2.2 Van der Waals

Van der Waals (VdW) forces are attractive intermolecular forces, weaker than Coulombic interactions, originating from the correlated motion of electrons in adjacent colloidal particles (Mitchell and Soga, 2005). Casimir and Polder (1948) showed that van der Waals pair-potential between two atoms for frequencies corresponding to wavelength lower than 10^3 Å = 100 nm = 0.1 µm is proportional to r^{-6}. For $r > 10^3$ Å, the pair potential is attenuated and proportional to r^{-7} (retardation effect). For short-range distance, van der Waals interaction energy between two atoms is given by:

$$U_{\mathrm{vdW,atoms}} = -\frac{3\alpha_0^2 h\nu}{4(4\pi\varepsilon_0)^2}\frac{1}{r^6} = -\frac{C}{r^6} \quad [7]$$

where r is the atomic separation distance, $\alpha_0 = 4\pi\varepsilon_0 R^3$ is the electronic polarizability of a one-electron atom of radius R, $\nu = 3.3\cdot10^{15}$ s^{-1} the orbiting frequency of the electron, h is the Planck constant, so that $h\nu = 2.2\cdot10^{-18}$ J is the energy needed to ionise the atom.

The interaction energies for pairs of different geometrical bodies can be derived from Eq.[7]. Under the assumption of additive interaction, one may integrate the interaction energy of all the atoms in one body with all the atoms in the other body. Let us consider two colloidal platelets. Assuming that the atoms of the two platelets are distributed according to two continuous functions of position ρ_1 and ρ_2, take two atoms i and j belonging to particle 1 and particle 2, respectively, with r_{ij} their separating distance and u_{ij} their pair potential, the total interaction potential can be written as:

$$U_{\mathrm{vdW}} = \int_{V_1}\int_{V_2} \rho_1\rho_2 u_{ij}(r_{ij})\,dV_1\,dV_2 \quad [8]$$

where V_1 and V_2 are the volumes of the two colloidal particles. Eq.[8] is written under the assumption that each atom is associated with the elementary mass ρ dV.

According to Hamaker (1937), $u_{ij}(r_{ij})$ is negative and, thus, attractive as the net force between colloidal particles is always attractive.

Eq. [8] has been solved for different geometries (Parsegian, 2006) in terms of the Hamaker constant:

$$A_H = \pi^2 C \rho_1 \rho_2 \quad [9]$$

Here, we consider the example of two finite square parallel platelets of negligible thickness (Figure 1).

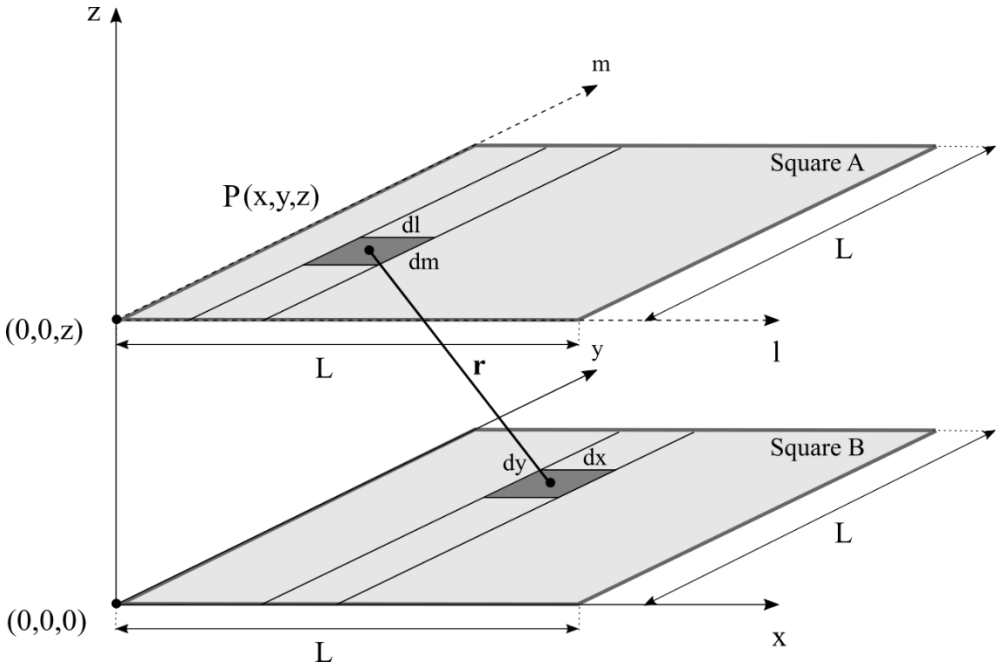

Figure 1. Schematic layout for analytic calculation of van der Waals interaction energy at any given relative particle orientation.

The attractive pair-energy between two squares A and B (Figure 1) with sides of length *L* separated by a vertical distance *z* can be computed by choosing a point P (*x*,*y*,*z*) on square A and calculating its energy potential with respect to square B. One can then integrate over *l* and *m* on square A. The distance between the point (*x*,*y*,*z*) on square A and square B is $r = \sqrt{x^2 + y^2 + z^2}$. Therefore, the vdW interaction energy potential between the two aligned squares can be computed as:

$$U_{\mathrm{vdW}} = -\frac{A_H}{\pi^2}\int_0^L dm \int_{-m}^{L-m} dy \int_0^L dl \int_{-l}^{L-l} \frac{1}{(x^2+y^2+z^2)^3}\,dx \sim \frac{1}{z^3} \quad [10]$$

After integration of Eq.[10], it is found that U_{vdW} roughly decays as $1/z^3$ and not as much as $1/z^6$ as in the case of atom-to-atom interaction.

The attractive pair interaction energy can be computed for any relative orientation between two square plate-like particles.

3 DLVO INTERACTION FOR ELEMENTARY PARTICLE CONFIGURATIONS

Based on the numerical/analytical solution of the governing equations in Section 2, this section presents the energy-separation relationship between two finite clay platelets for three elementary particle configurations: face-to-face, edge-to-face, and edge-to-edge. For the sake of simplicity, the mathematical formulation of the energy-separation function is derived by considering clay particles as rigid, finite, uniformly charged square platelets of infinitesimal thickness. The same computation could be easily performed with more complex geometries (such as hexagonal plate-like particles or prisms) and non-uniformly charged particles (it is possible, for instance, to account for positively charged particle edges and negatively charged particle surfaces). However, these analyses are out of the scope of this work.

The DLVO total interaction energy, U_t, is calculated as the sum of the electrostatic potential energy, U_{Edl}, and van der Waals interaction energy, U_{vdW}. The electrostatic potential energy, U_{Edl}, was numerically computed by a FE analysis using the commercial platform COMSOL Multiphysics ® v. 6.1. U_{Edl} was calculated for the three elementary configurations by imposing either constant surface charge or constant surface potential as a model boundary condition on the particle faces. The resulting six electrostatic pair-potential energy functions were then added to the van der Waals interaction energy that was calculated for each particle configuration according to Eq.[10].

3.1 Electrostatic free energy

Three different models were built in the FE platform COMSOL to compute the pair-wise electrostatic energy of each elementary configuration. For each model, two charged plates of finite size were placed in the central region of a boxlike domain at a given minimum inter-particle distance, h [nm], varying from 0 nm to 600 nm. The platelets were two squares of infinitesimal thickness with a dimension of L=1μm. Two different computations were run for each model: one at constant particle surface charge and one at constant particle surface potential. For the simulations at constant surface charge, the electric charge on the particle surface was chosen to be uniformly distributed and equal to q=-2·10^{-3} C/m^2.

On the other hand, when constant surface potential conditions were considered, the value of surface potential, ϕ_0, was set equal to 103 mV. The boundary conditions to solve the PB equation were as follows: (1) a Dirichlet boundary condition (DBC), ϕ=0, was imposed on all the six outer surface boundaries of the box domain; (2) a Dirichlet boundary condition, $\phi=\phi_0$, was imposed on the platelets surface when modelling constant surface potential, whereas a Neumann boundary condition (NBC), $-n\cdot\nabla\phi=q/\varepsilon$, was considered for the constant surface charge model, n being the outer normal vector. The electric potential, ϕ, around the charged plates in electrolyte solutions practically vanishes 300 nm outward from the plate surfaces for constant surface charge and constant surface potential. The parameters employed for all analyses are the ones listed in Table 1.

Table 1: Parameters employed in the FE COMSOL simulations to compute the electrostatic interaction energy.

Poisson-Boltzmann parameters	
ε_0 [$C^2 J^{-1} m^{-1}$]	$8.8542 \cdot 10^{-12}$
ε_r [-]	76.7
k [$N m K^{-1}$]	$1.38 \cdot 10^{-23}$
e [C]	$1.602 \cdot 10^{-19}$
n_0 [ion m^{-3}]	$1.2044 \cdot 10^{22}$
ν [-]	1
T [K]	293

Numerical implementation

The simulation box size was adapted for each specific case. The distance between the particle edge and the outer box boundary was set to 100nm. Preliminary sensitivity analysis showed that this distance is sufficiently large not to affect the system's free energy and, hence, the interaction force. The square particles were meshed with quadratic elements, having a side of 20 nm. The volume around the particles is meshed with tetrahedral elements, increasing size from the particles to the domain's boundary, with a maximum element growth rate of 1.2.

Analytical vs numerical for infinitely extended sheet

Figure 2 shows the preliminary validation of a 1D FE numerical solution against the rigorous solution of the PB equation derived by solving the 1D PB equation according to Verwey and Overbeek (1948) (via the numerical solution of an elliptic integral). The two solutions overlap, and the FE analysis was used to derive the electrical potential under 3D conditions.

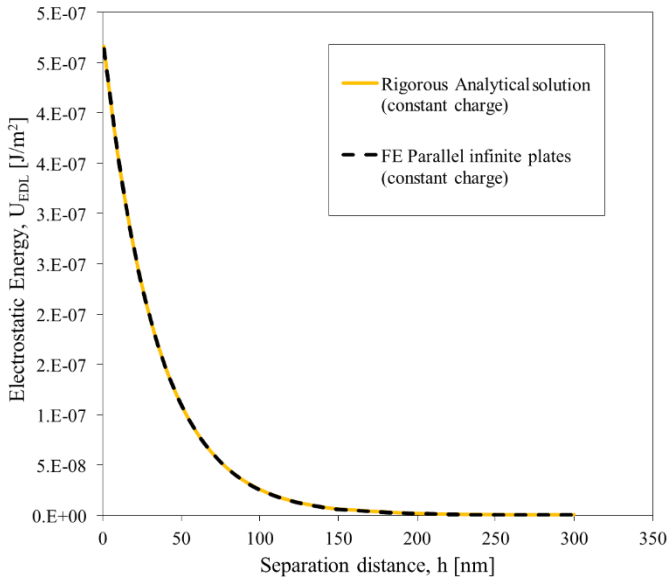

Figure 2. Validation of the finite element analysis for face-to-face infinite charged particles (1D) against the rigorous analytical solution according to Verwey and Overbeek (1948).

Elementary configuration: Face-to-face

Figure 3a shows the boxlike domain used for FE analyses of the face-to-face configuration of finite-size particles. Figure 3b presents the computed distribution of electrostatic free energy per unit area for increasing inter-particle distance at constant surface charge and potential. Additionally, in Figure 3b, the results were compared with the rigorous solutions for the parallel infinite plates of infinitesimal thickness.

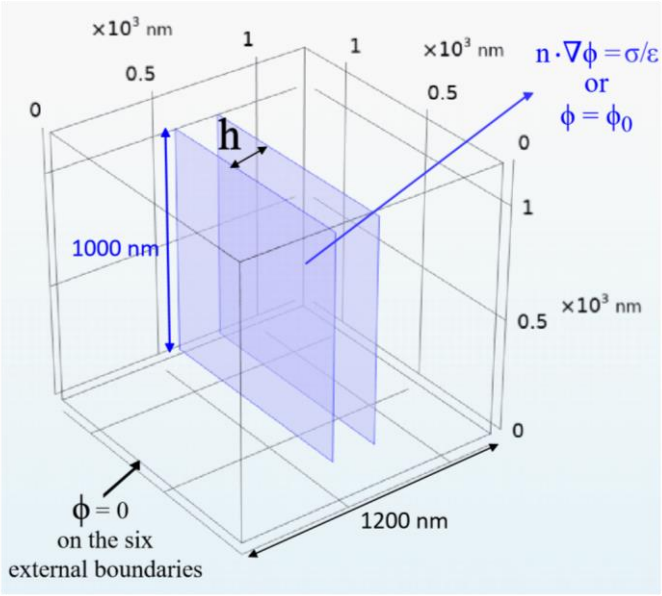

(a)

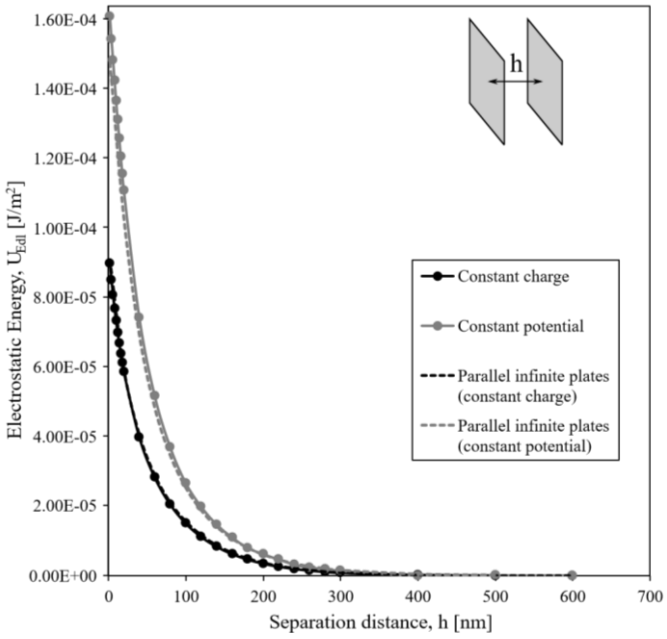

(b)

Figure 3. Finite element analysis for face-to-face particle configuration: (a) schematic diagram of the boxlike analysis domain and (b) potential energy vs minimum inter-particle distance at constant surface charge and surface potential. The dashed curves in (b) refer to the rigorous solutions; the continuous lines with markers represent the FE results.

A minimal difference exists between the two free energy distributions (finite and infinite plates) in face-to-face configuration (Figure 3b) for both constant surface charge and surface potential. This result is

intuitive as the plate dimensions of the finite particles are much larger than most of the considered inter-particle distances.

In such conditions, the finite plate behaves as 'infinitely wide' (the electrical field between the two opposing finite-size plates is essentially one-dimensional and practically coincides with the electrical field developing between infinitely wide plates). However, the effect of the particle's extremities may become non-negligible when inter-particle distance is of the same order of magnitude as the particle width.

Elementary configuration: edge to edge

The same procedure described for the face-to-face configuration was followed to compute the energy-separation curve in the edge-to-edge configuration (Figure 4). Once again, the distribution of U_{Edl} calculated numerically at constant surface charge and constant surface potential was compared with the rigorous solutions for two parallel infinite plates of infinitesimal thickness in Figure 4b. The interaction energy for edge-to-edge interaction of finite clay platelets is substantially smaller than the case of infinite plates.

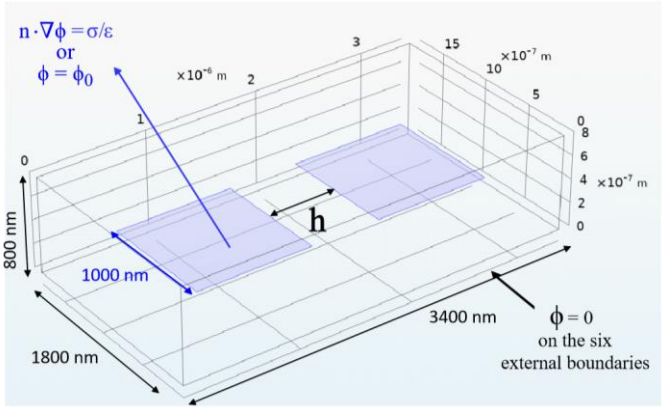

(a)

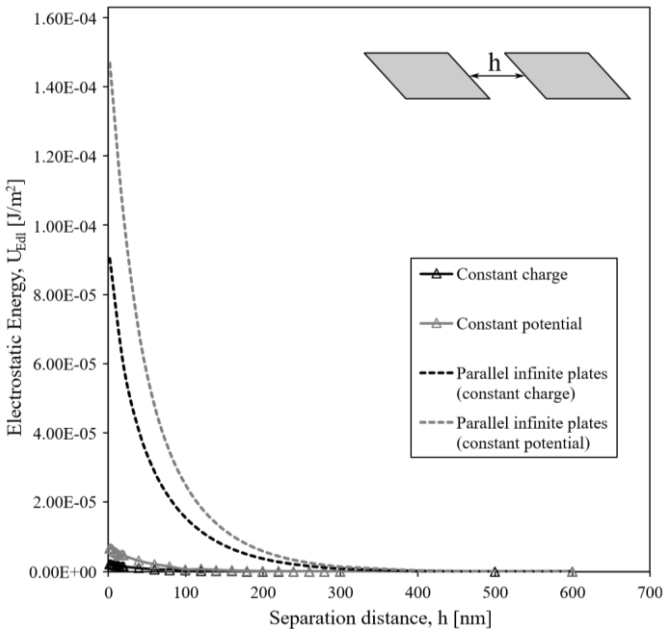

(b)

Figure 4. Finite element analysis for edge-to-edge particle configuration: (a) schematic diagram of the boxlike analysis domain and (b) potential energy vs minimum inter-particle distance at constant surface charge and surface potential.

Elementary configuration: edge to face

The same phenomenon can also be observed in Figure 5 for the edge-to-face configuration when the mutual particle inclination is α=90° (T-shape interaction). The interaction energy of finite particles in edge-to-face configuration is again smaller than the case of clay particles modelled as infinite parallel planar sheets of infinitesimal thickness.

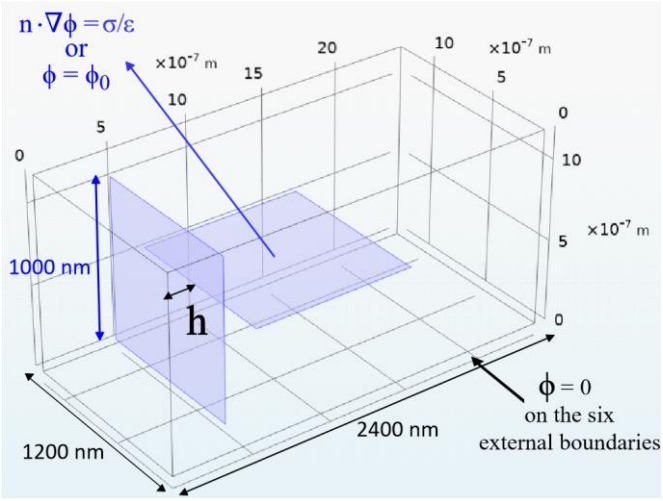

(a)

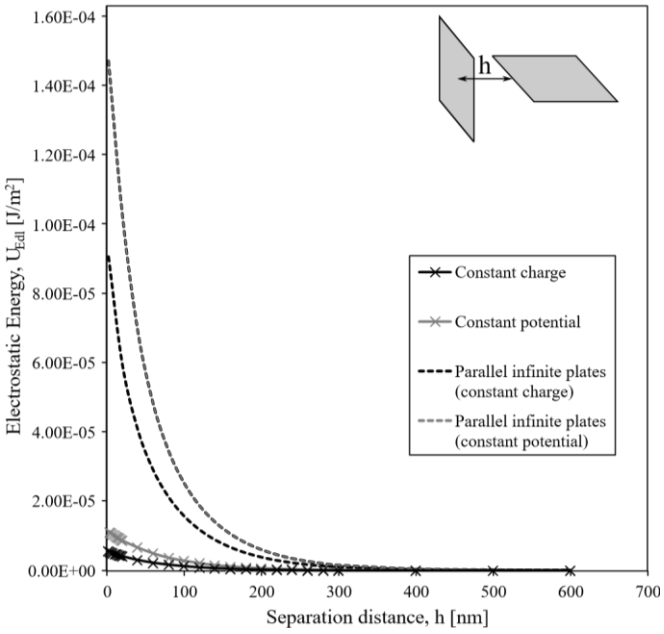

(b)

Figure 5. Finite element analysis for edge-to-face particle configuration: (a) schematic diagram of the boxlike analysis domain and (b) potential energy vs minimum inter-particle distance at constant surface charge and surface potential.

3.2 Van der Waals potential energy

The solution of Eq.[10] for the van des Waals potential energy for parallel aligned squares was computed analytically and is in line with the solution presented by De Rocco and Hoover (1960):

$$U_{vdW,FF} = -\frac{A}{\pi^2}\left[\frac{Lz^2+2L^3}{z^4\sqrt{L^2+z^2}}arctan\left(\frac{L}{\sqrt{L^2+z^2}}\right)-\frac{L}{z^3}arctan\left(\frac{L}{z}\right)\right] \quad [11]$$

Likewise, an analytical solution was also derived for two co-planar squares separated by a distance *z* (edge-to-edge configuration):

$$U_{vdW,EE} = -\frac{A}{\pi^2}\left[\frac{1}{48z^2}+\frac{z}{16L^2}arctan\left(\frac{z}{L}\right)+\frac{L}{16z^2}arctan\left(\frac{L}{z}\right)\right] \quad [12]$$

The computation of $U_{vdW,EF}$ for edge-to-face configuration is more complex as it requires the numerical solution of the integrals in Eq. [10]. The three van der Waals energy-separation curves are compared in Figure 6.

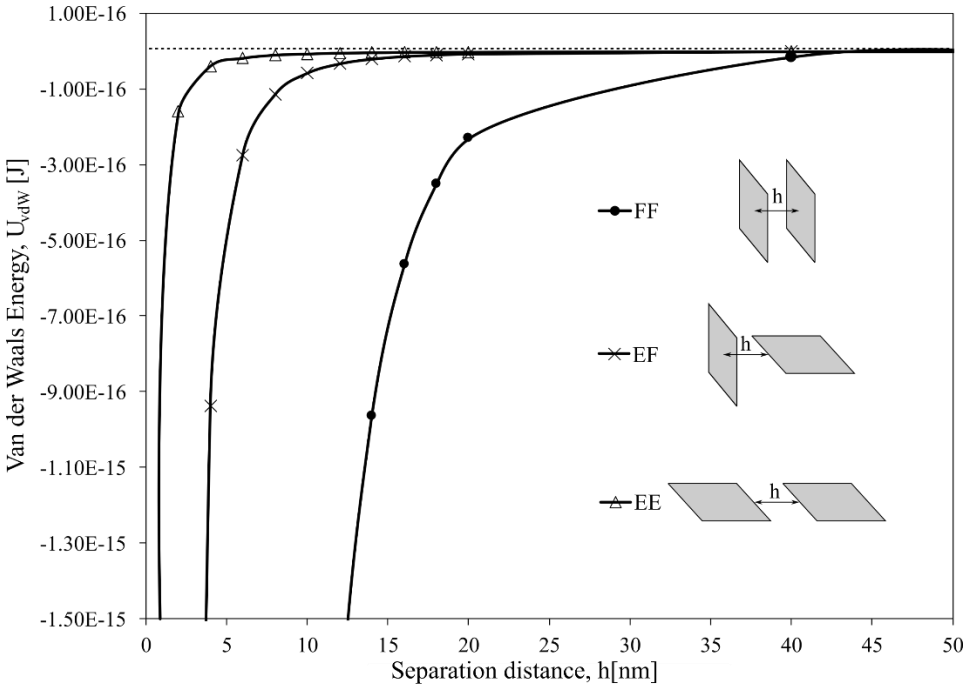

285

286 *Figure 6. Analytical calculation of van der Waals pair-energy interaction of two identical finite square platelets in face-to-*
287 *face, edge-to-edge and edge-to-face configuration.*

288 ## 3.3 DLVO-based energy-separation curves

289 Figure 7 presents the total energy-separation curves for two interacting finite square platelets of side
290 L=1μm in face-to-face, edge-to-edge and edge-to-face at constant surface charge (q=-2 mC/m^2) and
291 constant surface potential (ϕ_0=103 mV), respectively. The total energy curves are plotted against the
292 center-to-center distance, r, rather than the separation distance, h, for ease of comparison.

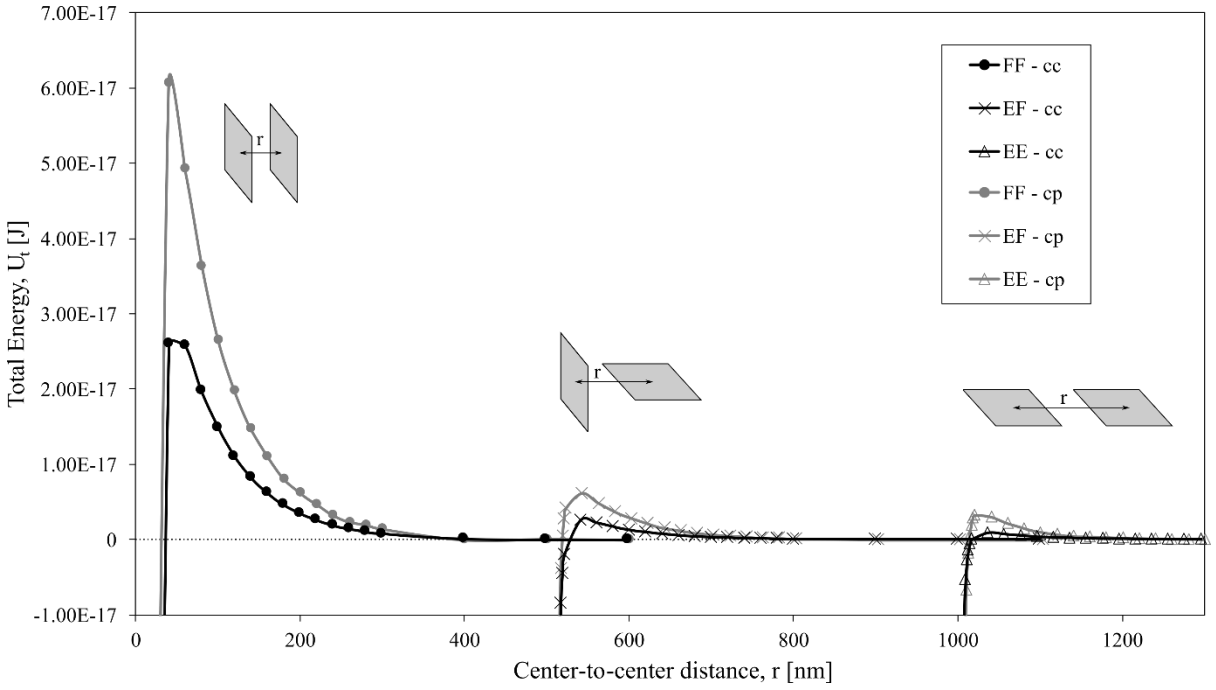

293

294 *Figure 7. Total energy-separation function for two interacting finite square platelets in face-to-face (FF), edge-to-face (EF)*
295 *and edge-to-edge (EE) configuration at constant surface charge (cc) and constant surface potential (cp).*

296 ## 3.4 Infinitesimal versus finite particle thickness

297 The choice of modelling clay particles with infinitesimal thickness was driven by the lack of an
298 analytical solution for the van der Waals interaction energy between two cuboidal particles randomly
299 oriented in space. The computation of the van der Waals potential energy for a pair of cuboidal particles
300 in a generic 3D configuration requires a sixfold integration (accounting for 2 particles and the 3
301 dimensions of the particles) of the interaction energy between two atoms (Eq. [7]). Considering square
302 particles of infinitesimal thickness reduces the number of integrals from 6 to 4 (Eq. [*10*]), making it
303 accessible for the numerical computation of interaction energy for a generic 3D configuration because
304 one dimension of the cuboidal particle (i.e., the thickness) vanishes.

305 To confirm the validity of this simplification, the DLVO interaction energy for two interacting identical
306 cuboidal particles of square cross-section (side L=1μm) and thickness t=L/100=10 nm was compared
307 to the results obtained for square platelets (side L=1μm) of infinitesimal thickness in FF and EE
308 configuration. This comparison is made possible by considering the analytical integration procedure De
309 Rocco and Hoover (1960) suggested for cuboidal particles in FF and EE configuration. An explicit

analytical formulation for two cuboids of square cross-section in FF configuration can be found in Casarella et al. (2024).

The DLVO total interaction energy, U_t, was then computed as the sum of the van der Waals interaction energy, $U_{vdW,}$ calculated according to De Rocco and Hoover (1960), and the electrostatic potential energy, U_{Edl}, numerically computed at constant surface charge or constant surface potential via the FE analysis in COMSOL. Figure 8 shows the boxlike half-domain implemented in COMSOL to compute the electrostatic potential energy of cuboidal particles in FF and EE configuration, Figure 8a and Figure 8b, respectively.

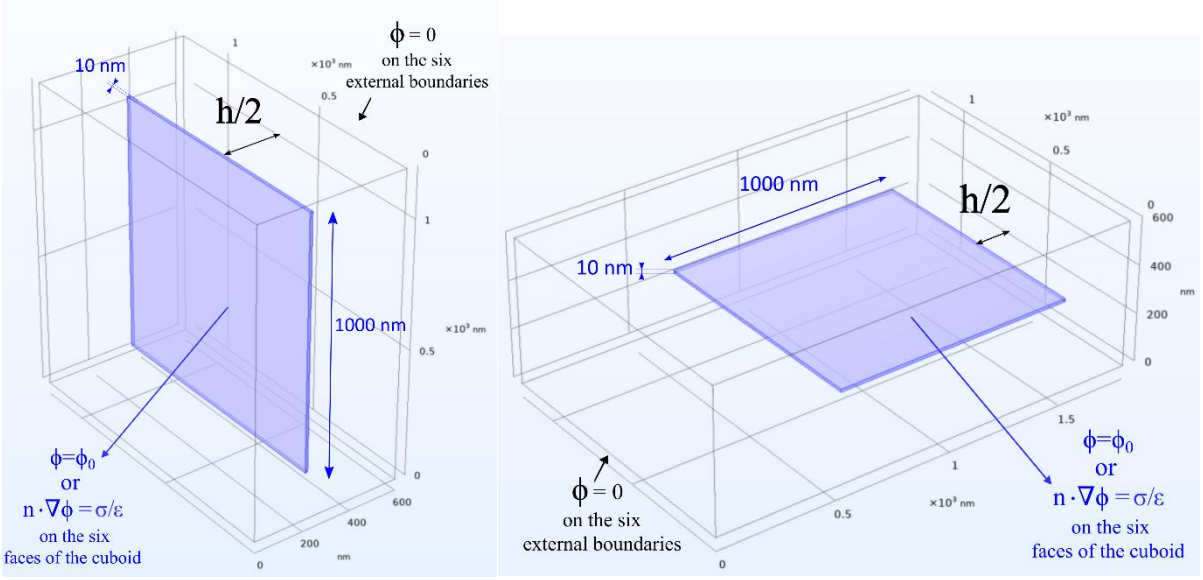

(a) *(b)*

Figure 8: Schematic diagram of the boxlike half-domain built in COMSOL for the finite element analysis of the electrostatic energy between two cuboidal platelets in (a) face-to-face (FF) and (b) edge-to-edge (EE) configuration.

The comparison between the DLVO total interaction energy when considering infinitesimal or finite thickness at constant surface charge and constant surface potential is shown in Figure 9. The plates with infinitesimal thickness were designed with either a constant surface potential of ϕ_0=-103 mV (both sides) or a surface charge of -2 mC/m^2 (-1 mC/m^2 per side). The cuboids were modelled either with a constant surface potential of ϕ_0=-103 mV on each face or a surface charge of -0.98 mC/m^2 on each of the six faces to match the total charge of the particles with infinitesimal thickness. The DLVO

interaction energy curves are plotted against the centre-to-centre distance, *r*, rather than the separation distance, *h*, for ease of comparison.

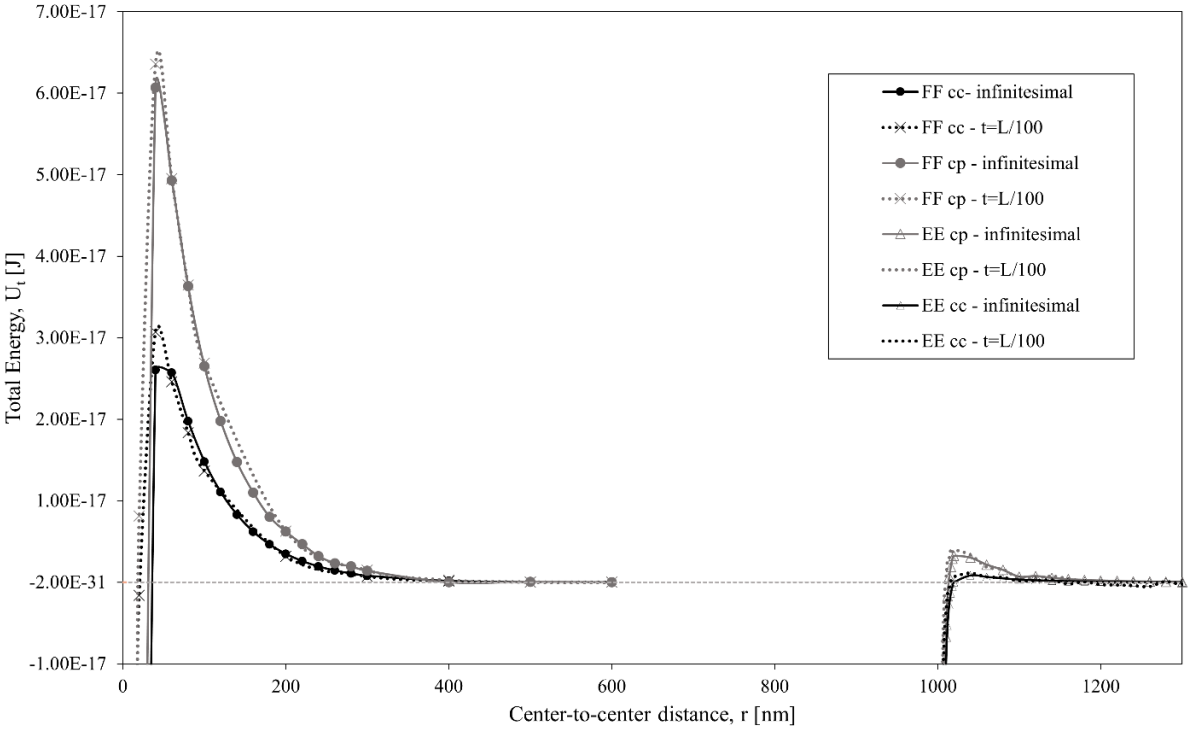

Figure 9: Comparison between the total energy-separation functions for two interacting finite square platelets and two interacting cuboidal particles of square cross-section in face-to-face (FF) and edge-to-edge (EF) configuration at constant surface charge (cc) and constant surface potential (cp).

The curves in Figure 9 are qualitatively and quantitatively very similar both at constant surface charge and constant surface potential. This result corroborates the choice of modelling the interaction energy by considering finite plates with infinitesimal thickness.

4 SQUARE PLATE VERSUS OBLATE ELLIPSOID

The energy-separation function has been derived for finite square plates of infinitesimal thickness. However, the energy-separation function for finite square plates will be used in this paper to calibrate and evaluate the Gay-Berne potential, which is formulated for ellipsoidal particles.

The EDL interaction energy and force were computed numerically for the case of an oblate ellipsoid ($a=b$ and $c=a/100$, Figure 10) and compared to the interaction energy derived for finite square plates.

The plate with infinitesimal thickness was designed with a side L=1μm=1000 nm and a surface charge of -2 mC/m^2 (-1 mC/m^2 per side). The oblate ellipsoid was designed with a surface charge of -1 mC/m^2 and the exact total charge to enable the comparison. The result is an oblate ellipsoid with dimensions of the semi-axes a=b=564 nm and c=5.64 nm. The ellipsoid was designed by assigning a constant relative dielectric permittivity to the material forming the particle, and two cases were considered, ε_r=5 and ε_r=80. The first value is typical of solid materials, while the second corresponds to the relative dielectric permittivity of the surrounding medium (aqueous electrolyte solution).

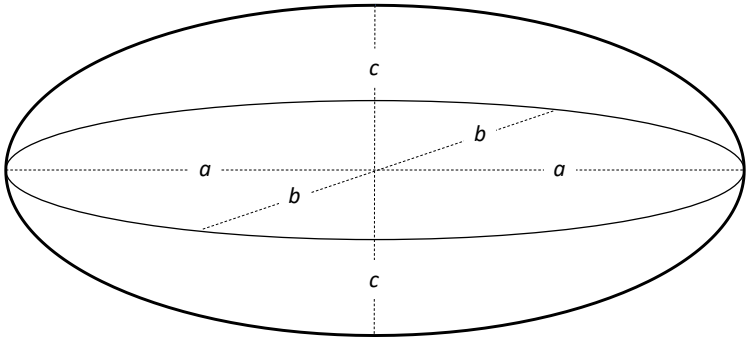

Figure 10. Ellipsoid geometry.

Figure 11a compares the finite plate and the oblate ellipsoid in terms of electrical double-layer free energy per unit projected area. The two curves are qualitatively similar, and there is a slight discrepancy due to the different geometry of the interacting elements. It is worth noting that the arbitrary assumption about the dielectric permittivity of the material forming the oblate ellipsoid does not affect the interaction energy of the oblate ellipsoids. Figure 11b shows the interaction force per unit area, where the discrepancy appears negligible. The electrostatic interaction pressure for infinite sheets at constant surface charge is also compared (p_{sheet}=σ^2/2ε, where σ [C/m^2] is the surface charge and ε [C^2/Jm] is the dielectric permittivity of the surrounding medium). As expected, the interaction force per unit area tends to be the interaction pressure for infinite sheets.

The results shown in Figure 11 corroborate the assumption that the interaction energy for oblate ellipsoidal particles can be assumed to be practically equal to the interaction energy of finite plates with infinitesimal thickness.

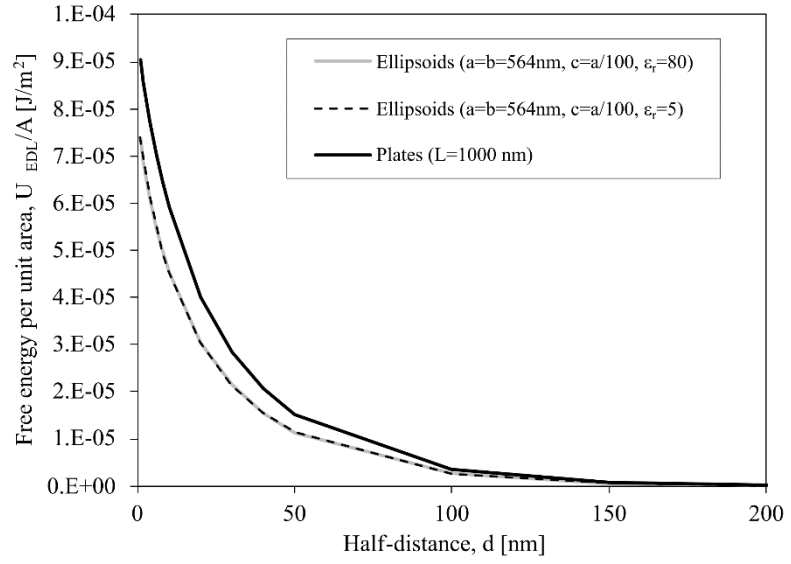

(a)

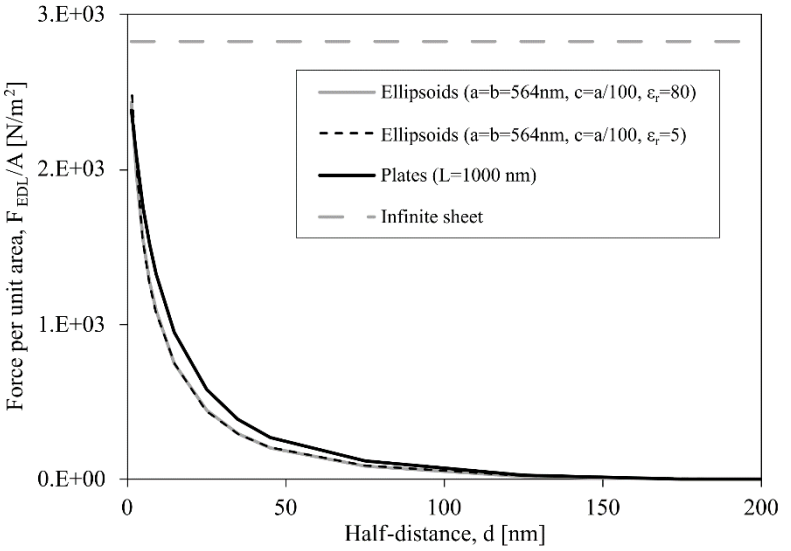

(b)

Figure 11. Comparison of infinitesimal thickness plate (L=1000 nm) and oblate ellipsoid (a=b=564 nm, c=a/100): (a) free energy per unit area; (b) force per unit area.

5 GAY-BERNE-TYPE POTENTIAL ENERGY

5.1 Gay-Berne potential

The Gay-Berne (GB) energy potential is a 3D modified form of the Lennard-Jones (LJ) energy potential (Lennard-Jones, 1931), and it was first introduced by Gay and Berne (1981) to evaluate the interaction of two rigid, ellipsoidal particles. The LJ energy potential (Figure 12) has been developed to

approximate the distance-dependent energy of interaction between a pair of spherical atoms/molecules in a fluid, *i* and *j*, respectively, as a function of the centre-to-centre distance, r_{ij}.

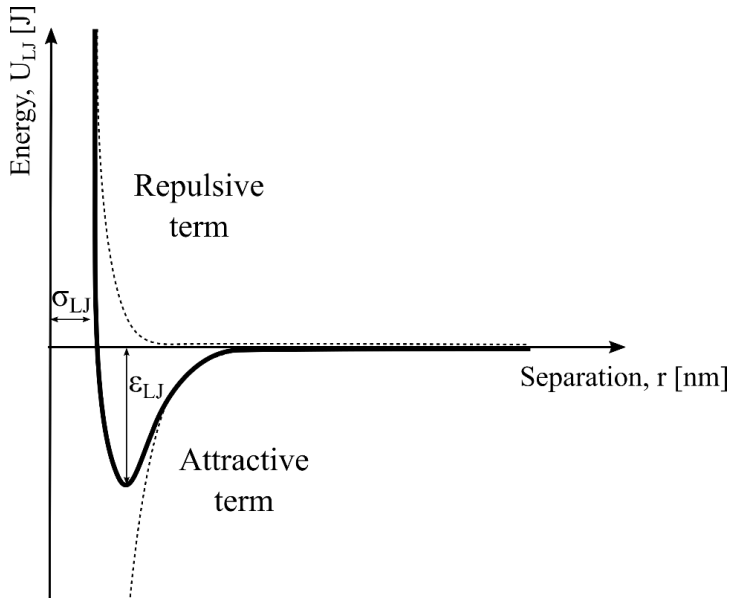

Figure 12. The typical shape of the Lennard-Jones 12-6 energy potential.

The LJ analytical form is given as follows:

$$U_{LJ}(r_{ij}) = 4\varepsilon_{LJ}\left[\underbrace{\left(\frac{\sigma_{LJ}}{r_{ij}}\right)^{12}}_{Born\ repulsion} - \underbrace{\left(\frac{\sigma_{LJ}}{r_{ij}}\right)^{6}}_{vdW\ attraction}\right] \quad [13]$$

where ε_{LJ} [J] denotes the depth of the attractive well and is related to the minimum of the potential energy function and σ_{LJ} [nm] is the separation distance at which the energy U_{LJ}=0. The total intermolecular pair potential comprises an attractive term ~$1/r^6$ and a repulsive term~$1/r^{12}$ (Eq.[13]).

In its original formulation, ~$1/r^{12}$ dominates at short distances and corresponds to the Born repulsion between the overlapping atom electron clouds. These repulsive forces are characterised by very short ranges and increase sharply as two molecules approach each other.

The attractive term ~$1/r^6$ represents the van der Waals contribution. According to the dispersion interaction energy between two identical atoms or molecules (London, 1936), the attractive energy decays as r_{ij}^{-6} in the non-retarded regime (Eq.[13]).

Since the potential decays asymptotically to zero at a considerable distance, the energy between particles is usually considered zero when the distance between them is more significant than a specific threshold value, which is called the cut-off distance and is denoted by r_{cut}. The truncation of the potential decreases the computational cost needed to perform a simulation by reducing the number of particles that each particle interacts with.

The Gay-Berne (GB) potential (Gay and Berne, 1981) can be seen as an anisotropic, 3D and shifted version of the LJ 12-6 interaction suitable for uniaxial (elongated) particles, where the LJ parameters, ε_{LJ} and σ_{LJ}, depend on the mutual orientation of the two units and their inter-particle vector.

Gay and Berne (1981) conducted several simulations to determine a new potential form specifically for non-spherical units, where the interaction energy depends on the minimum distance between these units and their relative orientation. They calibrated the pair-wise potential parameters from results obtained by considering face-to-face and edge-to-edge ellipsoids modelled as assemblies of spheres interacting according to the LJ potential. The resulting potential was further assessed for different particle orientations.

The GB potential presents several valuable numerical features. It can be easily differentiated analytically for the positional variables, avoiding the discontinuities of purely hard-core models. On the other hand, the version of the potential proposed by Gay and Berne (1981) is only appropriate for uniaxial (elongated) particles.

In this work, a generalised GB energy potential is considered for describing the interaction between pairs of dissimilar ellipsoidal particles (biaxial). The generalised GB energy potential is the one implemented in the MD software LAMMPS (Plimpton, 1995; Thompson et al., 2022), and it is given by the following functional form (Berardi et al., 1995; Everaers and Ejtehadi, 2003; Brown et al., 2009):

$$U_{GB}(\boldsymbol{R}_i, \boldsymbol{R}_j, \boldsymbol{r}_{ij}) = U_r(\boldsymbol{R}_i, \boldsymbol{R}_j, \boldsymbol{r}_{ij}, \gamma) \cdot \eta_{ij}(\boldsymbol{R}_i, \boldsymbol{R}_j, v) \cdot \chi_{ij}(\boldsymbol{R}_i, \boldsymbol{R}_j, \mu) \quad [14]$$

where $\boldsymbol{R}_i$ and $\boldsymbol{R}_j$ are the transformation matrices of the ellipsoid *I* and *j* describing the orientation in space of the two particles with respect to the simulation box frame; η_{ij} and χ_{ij} are dimensionless quantities that

represent the shape and energy anisotropies induced by the ellipsoidal shape of the considered units. U_r controls the site-to-site interaction as a function of the shortest distance between the two particles (h_{ij}), and it is defined as:

$$U_r = 4\varepsilon_{GB}\left[\left(\frac{\sigma_{GB}}{h_{ij}+\gamma\sigma_{GB}}\right)^{12} - \left(\frac{\sigma_{GB}}{h_{ij}+\gamma\sigma_{GB}}\right)^{6}\right] \quad [15]$$

where ε_{GB} [J] is the energy scale, σ_{GB} [nm] is a length scale, γ [-] is a dimensionless parameter that shifts the separation distance associated with the potential minimum and accounts for the particle'' finite radii. By definition, the parameter γ is related to the ellipsoid size. However, assuming it as a tunable model parameter is standard practice.

The distance of closest approach between two particles, h_{ij}, depends on their sizes and orientations and is defined by the following equation:

$$h_{ij} = \left|\boldsymbol{r_{ij}}\right| - \sigma_{GB,ij} \quad [16]$$

where $|\boldsymbol{r_{ij}}|$ [nm] is the centre-to-centre distance between the particles and $\sigma_{GB,ij}$ [nm] is defined as per Eq.[17], where the superscript T denotes the transpose matrix:

$$\sigma_{GB,ij} = \left(\frac{1}{2}\bar{\boldsymbol{r}}_{ij}^{T}\boldsymbol{G}_{ij}^{-1}\bar{\boldsymbol{r}}_{ij}\right)^{1/2} \quad [17]$$

with $\bar{\boldsymbol{r}}_{\boldsymbol{ij}}$ [-] being the normalised distance:

$$\bar{\boldsymbol{r}}_{ij} = \frac{\boldsymbol{r}_{ij}}{\left|\boldsymbol{r_{ij}}\right|} \quad [18]$$

and $\boldsymbol{G_{ij}}$:

$$\boldsymbol{G}_{ij} = \boldsymbol{R}_i^T\boldsymbol{S}_i^2\boldsymbol{R}_i + \boldsymbol{R}_j^T\boldsymbol{S}_j^2\boldsymbol{R}_j \quad [19]$$

where $\boldsymbol{S_i} = diag\ (a_i,b_i,c_i)$ and $\boldsymbol{S_j} = diag\ (a_j,b_j,c_j)$ are the diagonal shape matrices for particles i and j, respectively, and a, b, and c are the principal radii of the ellipsoidal particles. It is convenient to define a scalar value s characterising the geometry of the ellipsoid as a function of the semi-axis lengths:

$$s = (ab + cc)(ab)^{1/2} \quad [20]$$

The quantity η_{ij} depends on the particle'' dimensions and their relative orientation:

$$\eta_{ij} = \left(\frac{2s_i s_j}{det\boldsymbol{G}_{ij}}\right)^{v/2} \quad [21]$$

The exponent for the orientation-dependent shape function is v. This parameter has been empirically determined for liquid crystals, and a value of 1 was suggested by Berardi et al. (1995).

Likewise, the energy anisotropy χ_{ij} is computed using the following equation:

$$\chi_{ij} = \left(2\boldsymbol{r}_{ij}^T \boldsymbol{B}_{ij}^{-1} \boldsymbol{r}_{ij}\right)^{\mu} \quad [22]$$

where the following equation gives $\boldsymbol{B_{ij}}$:

$$\boldsymbol{B}_{ij}^{-1} = \boldsymbol{R}_i^T \boldsymbol{E}_i \boldsymbol{R}_i + \boldsymbol{R}_j^T \boldsymbol{E}_j \boldsymbol{R}_j \quad [23]$$

with $\boldsymbol{E}$=*diag*(ε_a, ε_b, ε_c) representing the energy matrix of each particle and ε_a, ε_b and ε_c the relative well depths, which are defined for three elementary configurations: face-to-face, edge-to-edge and side-to-side (Figure 13), respectively. The parameter μ has been empirically determined for liquid crystals, and a value of 2 was suggested by Berardi et al. (1995).

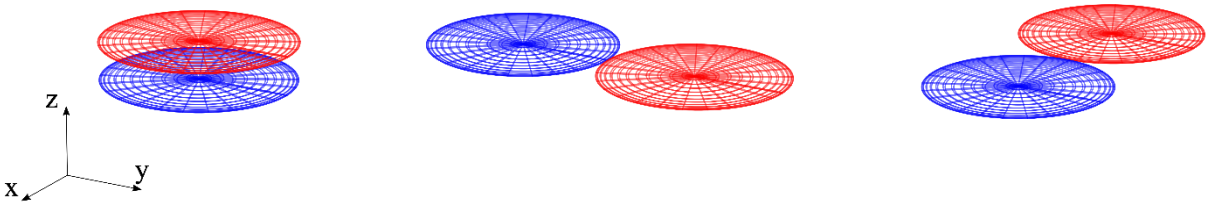

Figure 13. Face-to-face, edge-to-edge and side-to-side configurations of flat ellipsoids.

The shape and energy anisotropies η_{ij} and χ_{ij} depend on particle dimensions, their relative orientation, and the relative well-depth ($\varepsilon_{a,i}$, $\varepsilon_{b,i}$, $\varepsilon_{c,i}$, $\varepsilon_{a,j}$, $\varepsilon_{b,j}$, $\varepsilon_{c,j}$). When the ellipsoidal particles' radii are equal (a = b = c), the ellipsoid reduces to a sphere, and the shape anisotropy parameter η_{ij} equals 1. If one assumes

$\varepsilon_a = \varepsilon_b = \varepsilon_c$, the energy anisotropy parameter χ_{ij} also becomes equal to 1. With this specific parameter choice and considering γ=1, one obtains the original LJ formulation in Eq. [13].

The GB implementation described above is convenient as it allows simulations of a three-dimensional system containing ellipsoids of various aspect ratios interacting at different orientations. The formulation implemented in LAMMPS has been widely used for fully atomistic simulations of molecules and complex proteins. In soil mechanics, GB pair-wise potential has been employed by Ebrahimi et al. (2014) and Bandera et al. (2021) to simulate coarse-grained systems of montmorillonite and kaolinite, respectively.

5.2 'DLVO-adapted' Gay-Berne energy potential for CGMD modelling of clays

The LJ potential is the most widely used pair potential in Molecular Simulations. It is a reasonable choice for predicting atoms' and small molecules' contact energies and phase behaviour.

Conceptual discrepancies arise when employing the LJ potential (or the anisotropic 3D-version GB potential) in the Coarse-Grained (CG) modelling of colloidal particles. When the model elementary unit is one clay platelet of submicron length, the particle-particle interactions occurring at an atomic distance become negligible, and the relevant interaction distance goes from tens to a few hundred nanometers. Therefore, the very short-range Born repulsive forces (within a few nanometres) can be neglected. On the other hand, the long-range Coulombic repulsive forces arising from the particle net surface charge must be considered. The net particle interaction should be obtained by summing an attractive short-range term (van der Waals attraction) and a repulsive long-range term (Coulombic repulsion). Within the CG modelling of clay particles, the $\sim 1/r^{12}$ term of the LJ potential can now be used to model the attractive short-range van der Waals potential, whereas $\sim 1/r^{6}$ can be used to model the repulsive Coulombic branch (Figure 14).

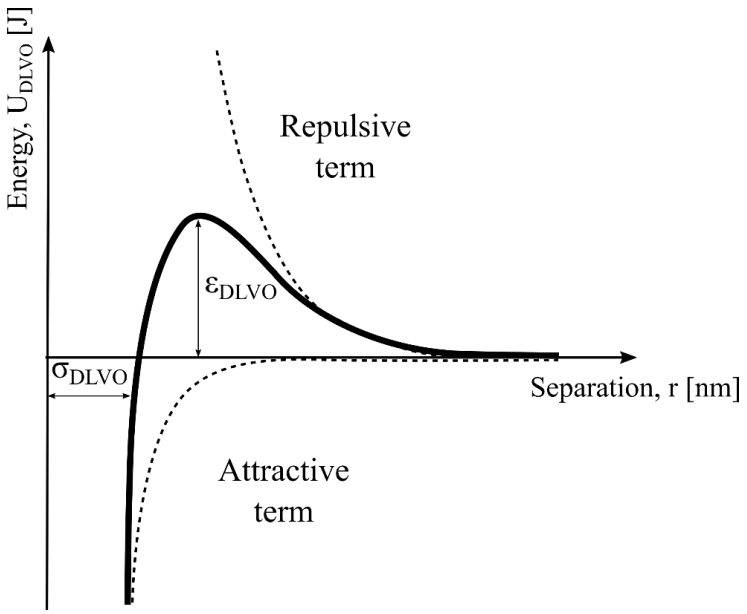

Figure 14. Adapted Lennard-Jones energy potential for CGMD modelling of clay particles.

This analytically translates in the following modification of Eq. [13]:

$$U_{DLVO}(r_{ij}) = -4\varepsilon_{DLVO}\left[\underbrace{\left(\frac{\sigma_{DLVO}}{r_{ij}}\right)^{12}}_{vdW\ attraction} - \underbrace{\left(\frac{\sigma_{DLVO}}{r_{ij}}\right)^{6}}_{Coulombic\ repulsion}\right] \quad [24]$$

Further to this change, the LJ can be employed to model the forces accounted for in the DLVO theory.

5.3 Generalised Gay-Berne energy potential (Mie potential) for CGMD modelling of clays

The choice of the two exponents 12 and 6 for the repulsive and attractive term in the original LJ pair energy potential was historically selected to model the molecular Born repulsion and van der Waals attraction, respectively. There is no evidence that the LJ 12-6 potentials are more efficient than other possible choices to simulate DLVO interaction between platy ellipsoidal particles. For example, the analysis of the vdW interaction of two parallel finite plates has shown that the vdW interaction energy is inversely proportional to the distance to the power of 3 (Eq. [10]) rather than the power of 6 as is the case of the 'original' Lennard-Jones potential or the power of 12 in the 'adapted' Lennard-Jones.

The Mie potential (Mie, 1903), for example, is as mathematically convenient as the LJ potential (power-law-based function) but allows for an arbitrary choice of the steepness of the decay of both the attractive and the repulsive term:

$$U_{MIE}(r_{ij}) = -4\varepsilon_{MIE}\left[\underbrace{\left(\frac{\sigma_{MIE}}{r_{ij}}\right)^{m}}_{vdW\ attraction} - \underbrace{\left(\frac{\sigma_{MIE}}{r_{ij}}\right)^{n}}_{Coulombic\ repulsion}\right] \quad [25]$$

with *m* and *n* integers.

6 CALIBRATION OF GB POTENTIAL AGAINST ELEMENTARY PARTICLE CONFIGURATION

The DLVO-adapted GB interaction energy between two identical disk-like particles requires seven parameters: one interaction distance parameter, σ_{DLVO} [nm], one energy parameter, $\varepsilon_{\mathrm{DLVO}}$ [J], two relative well depths, $\varepsilon_{a,\mathrm{DLVO}}$ (=$\varepsilon_{b,\mathrm{DLVO}}$) and $\varepsilon_{c,\mathrm{DLVO}}$ [-], the shift of the potential minimum γ_{DLVO} [-], the 'orientation' parameter ν (Eq. [21]), and the anisotropy parameter μ (Eq. [22]).

The MIE interaction energy model requires two additional parameters, *m* and *n* (Eq. [25]), for a total of 9 parameters.

It should be noticed that the well depths ε_a and ε_b, associated with the edge-to-edge interactions in two orthogonal directions, are assumed to be equal. As observed at the electron microscope, clay particles are approximately equidimensional in the basal plane a-b (Brown et al., 2009; Pedrotti and Tarantino, 2018a), and this leads to a representation of the clay particle as an oblate ellipsoidal geometry (Cadene et al., 2005) with two equal principal radii *a* and *b*, in turn, two orders of magnitude larger than the third radius, i.e., the thickness *c* (disc-like platelets).

The parameters of the DLVO-adapted GB and MIE potentials do not have a clear physical meaning, and they need to be calibrated against a known pair potential energy field. To this end, the diameter of the oblate ellipsoid platelets was set equal to the side of the square plates employed for the DLVO energy computation in the previous section. The elementary units chosen for the computation of the

DLVO-adapted and MIE potentials were platy rigid ellipsoids, with one semi-axis being two orders of magnitude smaller than the other two (a=b=500nm and c=5nm).

Two approaches were examined to calibrate the parameters of the 'DLVO-adapted' and MIE potentials depending on whether the 'orientation' parameter, ν, and the anisotropy parameter, μ, were pre-selected based on the literature or were best fitted.

Approach 1 - Orientation and anisotropy parameters set to ν=1 and μ=2

Following Berardi et al. (1995), Ebrahimi et al. (2014) and Bandera et al. (2021), the 'DLVO-adapted' GB potential and MIE potential were calibrated against the separation-energy relationship for two elementary interactions only, edge-to-edge and face-to-face, derived according to the DLVO framework presented in Section 3. The model parameters, μ and ν, were also fixed and assumed equal to 2 and 1, respectively (Berardi et al., 1995; Ebrahimi et al., 2014; Bandera et al., 2021). The five model parameters for the 'DLVO-adapted' GB potential (ε_{DLVO}, γ_{DLVO}, σ_{DLVO}, $\varepsilon_{a,DLVO}$ and $\varepsilon_{c,DLVO}$) and the seven model parameters for the MIE potential (ε_{MIE}, γ_{MIE}, σ_{MIE}, $\varepsilon_{a,MIE}$ and $\varepsilon_{c,MIE}$, m, and n) were then adjusted by fitting Eqs.[24] and [25] against the energy-separation curves determined for these two elementary interactions. It should be noted that the constraint $m/n = 2$ was imposed on the MIE potential.

Table 2 summarises the calibrated parameters for Approach 1 (μ=2 and ν=1) for constant surface charge and constant surface potential. Figure 15 presents the calibration of the GB potential using Approach 1. Since only face-to-face and edge-to-edge DLVO data were used for calibration, the edge-to-face curves (Figure 15b and Figure 15e) can be viewed as a genuine prediction simulation. 'DLVO-adapted' GB and MIE potentials simulation of edge-to-face potential appears relatively poor. It appears that the MIE potential (m=3 and n=1.5) reproduces the decay of the electrostatic repulsion better than the 'DLVO-adapted' GB potential (m=12 and n=6).

Approach 2 - Orientation and anisotropy parameters ν and μ by best fitting

Zannoni (2018) explicitly specifies that the parameterisation μ=2 and ν=1 proposed by Berardi et al. (1995) favours side-to-side interaction, in the sense that the well-depth in edge-to-edge configuration

522 turns out to be much higher than the well-depth in edge-to-face configuration. However, an opposite
523 trend appears from the three DLVO pair-interaction energy curves calculated in Figure 16, i.e., the well-
524 depth in edge-to-face configuration is higher than the well-depth in edge-to-edge configuration.
525 Employing the parameterisation proposed by Berardi et al. (1995) in a CGMD simulation of clay
526 particles would lead to an excessively low energy barrier in edge-to-face configuration and generate
527 diffuse edge-to-face contacts at the sample generation stage and upon mechanical loading.

528 Fundamental macroscopic phenomena observed in clay have been explained by looking at the micro-
529 mechanisms occurring at the edge-to-face particle interaction, such as the plastic response under
530 mechanical compression (Pedrotti and Tarantino, 2018a) and plastic contraction upon thermal loading
531 (Casarella et al., 2020). Underestimating the energy barrier at the edge-to-face contact means an
532 improper portrayal of the observed macroscopic response of clay and, thus, unrealistic predictions of
533 clay behaviour under experimentally unexplored paths.

534 To prevent this artefact, the parameters μ and ν were 'unlocked' and best-fitted together with the other
535 five parameters for both the 'DLVO-adapted' GB and the MIE potential (*m* and *n* were maintained
536 equal to 3 and 1.5, respectively, in the MIE potential). In this case, the seven parameters were fitted
537 against three elementary configurations: face-to-face, edge-to-edge, and edge-to-face. Table 3
538 summarises the parameters calibrated for the 'DLVO-adapted' GB and the MIE potentials for constant
539 surface charge and constant surface potential. Figure 16 compares the calibrated potentials with the
540 DLVO numerical data. As for approach 1, it appears that the MIE potential (*m*=3 and *n*=1.5) reproduces
541 better the decay of the electrostatic repulsion compared to the 'DLVO-adapted' GB potential (*m*=12
542 and *n*=6). In this case, the edge-to-face configuration is better reproduced.

543

544

545

546

547

548 *Table 2. Calibrated parameters for Approach 1.*

DLVO-adapted parameter	Value
γ_{DLVO} [-]	0.84
ε_{DLVO} [J]	6.75E-22
σ_{DLVO} [nm]	135
$\varepsilon_{a,DLVO} = \varepsilon_{b,DLVO}$ [-]	26
$\varepsilon_{c,DLVO}$ [-]	850
ν [-]	1
μ [-]	2

549 *(a) 'DLVO-adapted' GB (m=12, n=6) - cc.*

MIE parameter	Value
γ_{MIE} [-]	0.27
ε_{MIE} [J]	6.75E-22
σ_{MIE} [nm]	28
$\varepsilon_{a,MIE} = \varepsilon_{b,MIE}$ [-]	26
$\varepsilon_{c,MIE}$ [-]	850
ν [-]	1
μ [-]	2

550 *(b) MIE (m=3, n=1.5) - cc.*

DLVO-adapted parameter	Value
γ_{DLVO} [-]	0.88
ε_{DLVO} [J]	1.68E-21
σ_{DLVO} [nm]	130
$\varepsilon_{a,DLVO} = \varepsilon_{b,DLVO}$ [-]	40
$\varepsilon_{c,DLVO}$ [-]	740
ν [-]	1
μ [-]	2

551 *(c) 'DLVO-adapted' GB (m=12, n=6) - cp.*

MIE parameter	Value
γ_{MIE} [-]	0.3
ε_{MIE} [J]	1.68E-21
σ_{MIE} [nm]	24
$\varepsilon_{a,MIE} = \varepsilon_{b,MIE}$ [-]	40
$\varepsilon_{c,MIE}$ [-]	740
ν [-]	1
μ [-]	2

552 *(d) MIE (m=3, n=1.5) - cp.*

553

554 *Table 3. Calibrated parameters for Approach 2.*

DLVO-adapted parameter	Value
γ_{DLVO}[-]	0.84
ε_{DLVO} [J]	2.82E-20
σ_{DLVO} [nm]	135
$\varepsilon_{a,DLVO} = \varepsilon_{b,DLVO}$ [-]	26
$\varepsilon_{c,DLVO}$ [-]	850
ν [-]	0.05
μ [-]	4

555 *(a) 'DLVO-adapted' GB (m=12, n=6) - cc.*

MIE parameter	Value
γ_{MIE} [-]	0.27
ε_{MIE} [J]	2.82E-20
σ_{MIE} [nm]	28
$\varepsilon_{a,MIE} = \varepsilon_{b,MIE}$ [-]	26
$\varepsilon_{c,MIE}$ [-]	850
ν [-]	0.05
μ [-]	4

556 *(b) MIE (m=3, n=1.5) - cc.*

DLVO-adapted parameter	Value
γ_{DLVO}[-]	0.88
ε_{DLVO} [J]	4.38E-20
σ_{DLVO} [nm]	130
$\varepsilon_{a,DLVO} = \varepsilon_{b,DLVO}$ [-]	40
$\varepsilon_{c,DLVO}$ [-]	740
ν [-]	0.175
μ [-]	7

557 *(c) 'DLVO-adapted' GB (m=12, n=6) - cp.*

MIE parameter	Value
γ_{MIE} [-]	0.36
ε_{MIE} [J]	4.38E-20
σ_{MIE} [nm]	24
$\varepsilon_{a,MIE} = \varepsilon_{b,MIE}$ [-]	40
$\varepsilon_{c,MIE}$ [-]	740
ν [-]	0.175
μ [-]	7

558 *(d) MIE (m=3, n=1.5) - cp.*

559

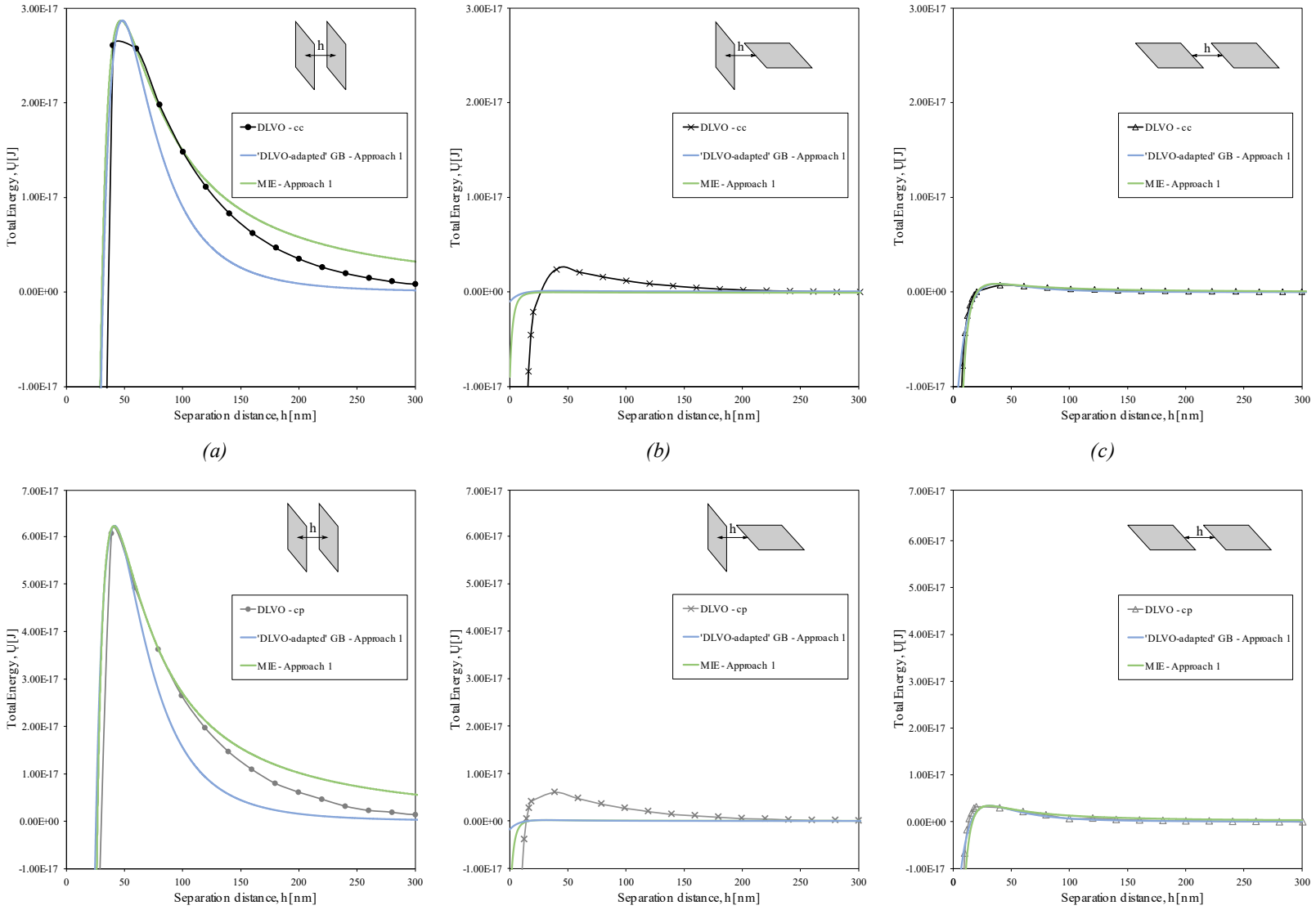

Figure 15. Approach 1: calibration of the 'DLVO-adapted' GB and MIE potentials against the DLVO energy-separation distance relationships for finite square platelets at constant surface charge (a), (b) and (c) and constant surface potential (d), (e) and (f) (figures (b) and (e) can be considered as a prediction as they were not used for calibration).

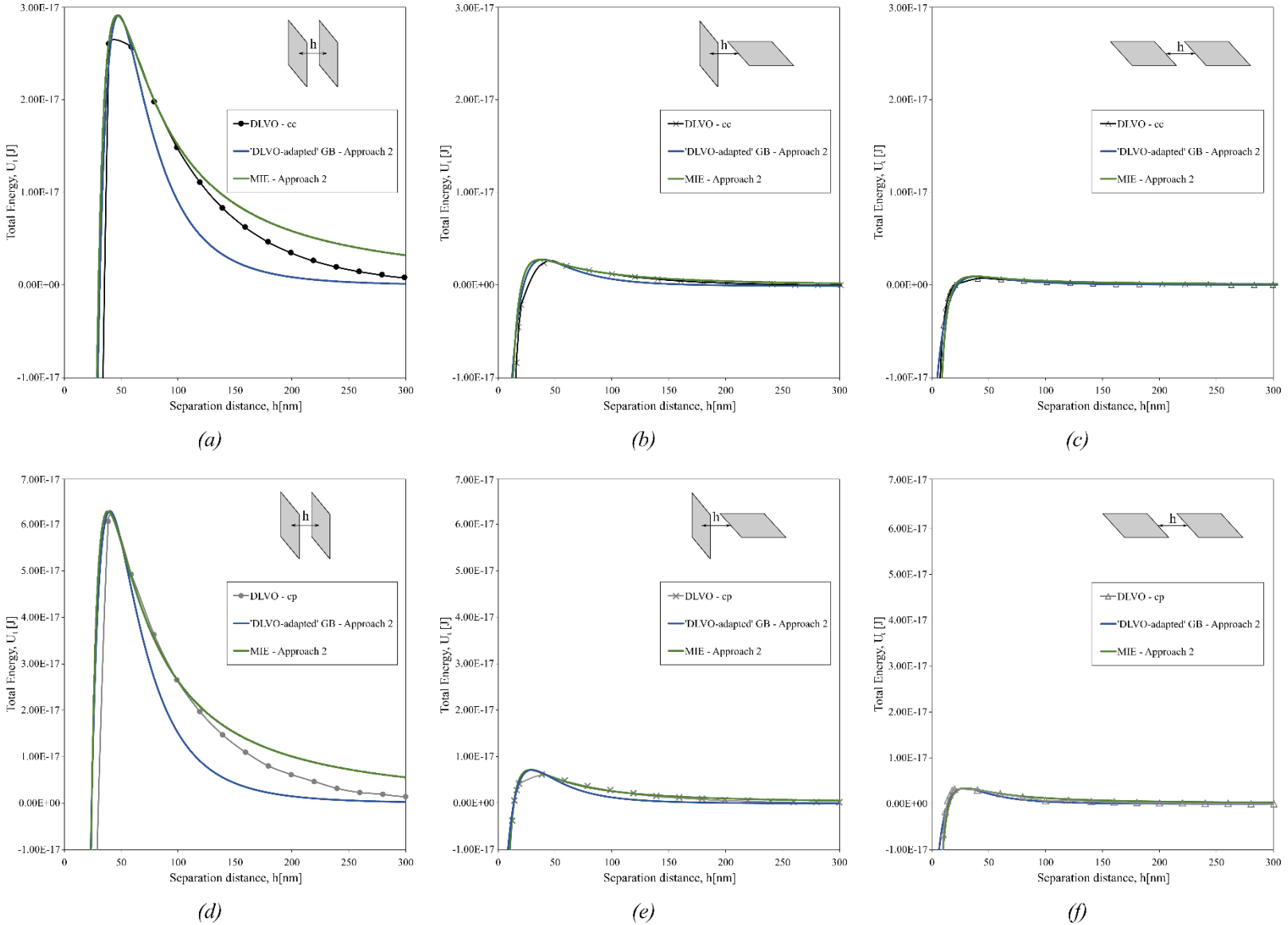

Figure 16. Approach 2: calibration of the 'DLVO-adapted' GB and MIE potentials against the DLVO energy-separation distance relationships for finite square platelets at constant surface charge (a), (b) and (c) and constant surface potential (d), (e) and (f).

7 EVALUATION AGAINST GENERIC PARTICLE CONFIGURATION

The 'DLVO-adapted' GB and MIE potentials are designed to represent the interaction energy for any generic configuration once their parameters are calibrated against elementary modes of interaction. To assess their performance, the simulations of the 'DLVO-adapted' GB and MIE potentials based on the parameters calibrated for the case of constant charge (Table 2a, Table 2b, Table 3a and Table 3b) were compared to DLVO numerical data in Figure 17. Four generic diverse configurations were selected for the validation. Validation case A (Figure 17a and Figure 17b) consists of a non-parallel face-to-face configuration with a relative orientation equal to 45° around the y-axis. Moreover, when the separation distance *h* approaches 0, the edges of the two particles come into contact. Validation case B (Figure 17c and Figure 17d) consists of a 'skew' edge-to-face configuration with a relative orientation equal to 70° around the y-axis and 30° around the z-axis. In this case, the particles have a point contact at small separation distances. Validation case C (Figure 17e and Figure 17f) includes two skewed parallel squares with a relative orientation equal to 30° around the z-axis. The two particles are in face-to-face configuration, but the projected areas overlap by only 42%. Validation case D (Figure 17g and Figure 17h) consists of a 'skew' edge-to-edge configuration with a relative orientation equal to 10° around the y-axis and 30° around the z-axis. In this case, the projected areas do not overlap.

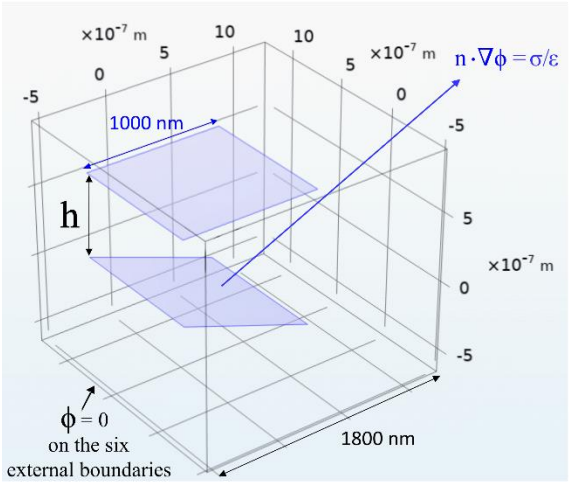
×10⁻⁷ m
n·∇ϕ = σ/ε
1000 nm
h
ϕ = 0
on the six
external boundaries
1800 nm

582

(a)

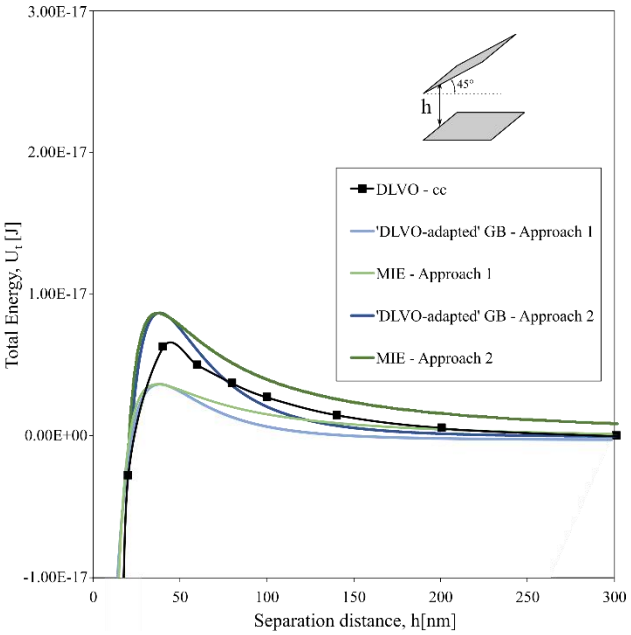
Total Energy, U_t [J]
Separation distance, h[nm]
h
45°
DLVO - cc
'DLVO-adapted' GB - Approach 1
MIE - Approach 1
'DLVO-adapted' GB - Approach 2
MIE - Approach 2

(b)

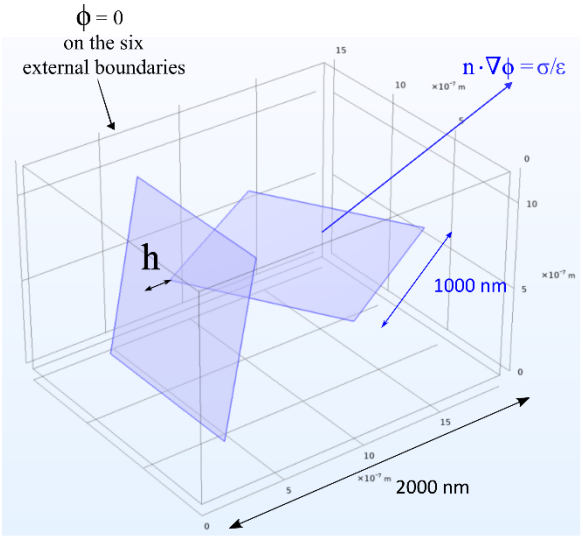
ϕ = 0
on the six
external boundaries
n·∇ϕ = σ/ε
h
1000 nm
2000 nm

583

(c)

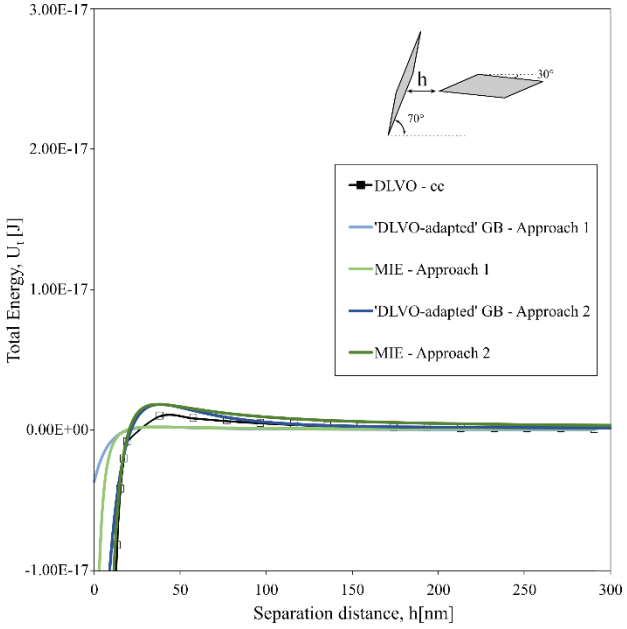
Total Energy, U_t [J]
Separation distance, h[nm]
h
30°
70°
DLVO - cc
'DLVO-adapted' GB - Approach 1
MIE - Approach 1
'DLVO-adapted' GB - Approach 2
MIE - Approach 2

(d)

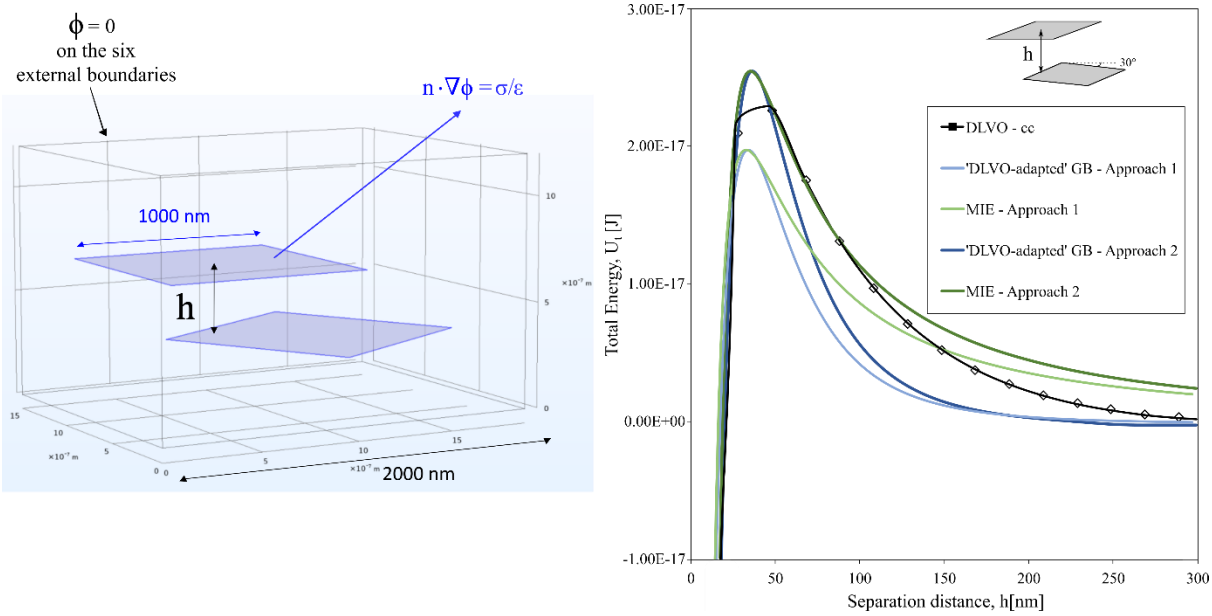

584

(e) *(f)*

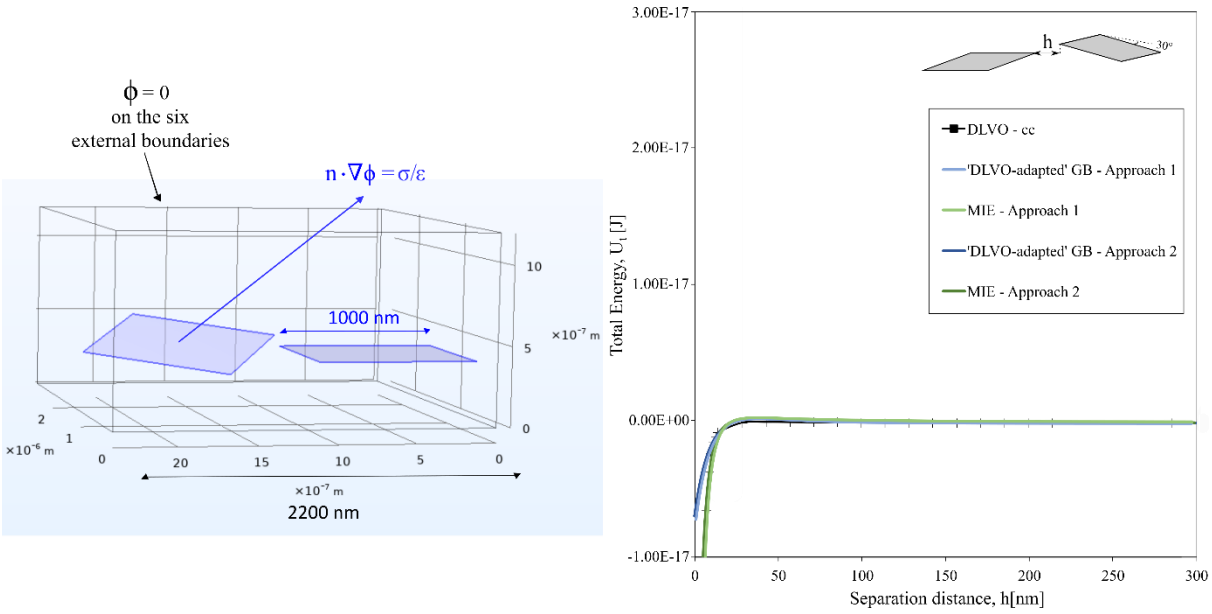

585

(g) *(h)*

586 *Figure 17. Evaluation of the 'DLVO-adapted' GB and MIE potentials against the DLVO energy-separation distance*
587 *relationship for finite square platelets at constant surface charge in three generic configurations. Validation case A - mutual*
588 *inclination between the two squares equal to 45° around the y-axis: (a) schematic diagram of the analysis domain in COMSOL*
589 *and (b) potential energy vs separation distance. Validation case B - mutual inclination between the two squares equal to 70°*
590 *around the y-axis and 30° around the z-axis: (c) schematic diagram of the analysis domain in COMSOL and (d) potential*
591 *energy vs separation distance. Validation case C – skewed face-to-face squares with a mutual inclination of 30° around the z-*
592 *axis: (c) schematic diagram of the analysis domain in COMSOL and (d) potential energy vs separation distance. Validation*

case D – skewed edge-to-edge squares with a mutual inclination of 10° around the y-axis and 30° around the z-axis: (c) schematic diagram of the analysis domain in COMSOL and (d) potential energy vs separation distance.

The 'DLVO-adapted' GB and MIE simulation curves agree with the DLVO numerical data (Figure 17b, Figure 17d, Figure 17f, and Figure 17h) for the case of μ and v unlocked (Approach 2). Additionally, it can be seen, for example, in Figure 17d that Approach 2 (both 'DLVO-adapted' GB and MIE formulations) captures the qualitative decrease in the energy barrier when particles move from face-to-face configuration (relative particle orientation around the y-axis equal to 0°) to edge-to-face configuration (relative particle orientation around the y-axis equal to 90°). However, in all the validation cases, the 'DLVO-adapted' GB and MIE potentials overestimate the energy barrier by around 25% (average on the four validation cases presented).

Despite this discrepancy, the 'prediction' of the 'DLVO-adapted' GB and MIE potentials for generic configurations appears to be satisfactory, provided the 'DLVO-adapted' GB and MIE potentials are calibrated based on seven parameters (i.e., including μ and v as per Approach 2). On the contrary, the 'prediction' of the 'DLVO-adapted' GB and MIE potentials for the calibration against five parameters (Approach 1, μ=2 and v=1) appears relatively poor.

8 CONCLUSIONS

This paper has first presented DLVO-based energy-separation curves for a pair of finite platy particles in three elementary configurations: face-to-face, edge-to-edge, and edge-to-face, respectively. Following the DLVO theory, the novel dataset was generated by summing the electrostatic interaction energy, U_{Edl}, and the van der Waals interaction energy, U_{vdW}, between two finite uniformly charged square platelets of infinitesimal thickness. The electrostatic component was computed numerically by solving the non-linear 3D Poisson-Boltzmann equation with the Finite Element (FE) method. The short-range van der Waals energy was calculated analytically.

This dataset can inform qualitatively and quantitatively the constitutive energy/force separation functions in DEM and CGMD modelling. The advantage of using the DLVO framework is that it embeds the combined effect of temperature, dielectric permittivity, and electrolyte concentration of the

pore fluid. Therefore, it can underpin the modelling of clay mechanical behaviour associated with thermal and environmental loading.

In this study, the Gay-Berne potential, as implemented in the open-source MD code LAMMPS, was calibrated and evaluated against the DLVO free energy data for the three elementary configurations (face-to-face, edge-to-face and edge-to-edge). The Gay-Berne potential may be considered a three-dimensional version of the Lenard-Jones potential used to characterise the interaction between two atoms/molecules. Two versions of the Gay-Berne potential were considered:

- 'DLVO -adapted' Gay-Berne potential where i) the Born repulsion branch of the original Lennard-Jones potential is used to represent the van der Waals attraction (by changing the sign of this energy term) and ii) the van der Waals repulsion branch of the original Lennard-Jones potential is used to represent the Columbic repulsion (by changing the sign of this energy term);
- MIE potential where the exponents m and n controlling the variation of the two energy terms forming the interaction potential are 'unlocked' (instead of assuming m=12 and n=6 as per the original Lennard-Jones potential).

The calibration procedure was performed for DLVO free energy curves computed at constant surface charge and constant surface potential. It has been shown that the orientation parameter, μ, and the anisotropy parameter, v, set to μ=2 and v=1 as adopted in CGMD clay modelling, favour side-to-side interaction and widely underestimate the energy required to bring edge-to-face particles in contact as predicted by the DLVO theory. On the other hand, μ=7 and v=0.175 capture adequately the progression of the shape of the pair energy-separation function when moving from face-to-face to edge-to-face and edge-to-edge configuration.

It has also been shown that the MIE potential (exponents m=3 and n=1.5) better captures the slow decay of the electrostatic repulsive energy component of the DLVO potential energy Coulombic branch of the interaction potential compared to the DLVO-adapted GB potential, which embeds the Lennard-Jones (LJ) exponents m=12 and n=6.

ACKNOWLEDGEMENTS

This work was funded by the ANR project GEO2 (ANR-19-CE05-0003-01). The laboratory 3SR is part of the LabEx Tec 21 (Investissement d'avenir – grant agreement n. ANR-11-LABX-0030).

DATA AVAILABILITY STATEMENT

Some or all data, models, or code that support the findings of this study are available from the corresponding author upon reasonable request.

REFERENCES

Bandera, S., O'Sullivan, C., Tangney, P., and Angioletti-Uberti, S. (2021). Coarse-grained molecular dynamics simulations of clay compression. Computers and Geotechnics, 138:104-333. https://doi.org/10.1016/j.compgeo.2021.104333

Berardi, R., Fava, C., and Zannoni, C. (1995). A generalised gay-berne intermolecular potential for biaxial particles. Chemical Physics Letters, 236:462–468. https://doi.org/10.1016/0009-2614(95)00212-M

Brown, W. M., Petersen, M. K., Plimpton, S. J., and Grest, G. S. (2009). Liquid crystal nanodroplets in solution. Journal of Chemical Physics, 130(4):1–7. https://doi.org/10.1063/1.3058435

Casarella, A., Tarantino, A., and Di Donna, A. (2020). Micromechanical interpretation of thermo-plastic behaviour of clays. In E3S Web of Conferences (Vol. 205, p. 09003). EDP Sciences. https://doi.org/10.1051/e3sconf/202020509003

Casarella, A., Tarantino, A., & di Donna, A. (2024). Revisiting DLVO theory to inform particle-scale modelling of clays. Computers and Geotechnics, 165, 105876. https://doi.org/10.1016/j.compgeo.2023.105876

COMSOL Multiphysics® v. 6.1. www.comsol.com. COMSOL AB, Stockholm, Sweden.

666 Casimir, H. B. G. and Polder, D. (1948). The influence of retardation on the London-van der Waals
667 forces. Phys. Rev., 73:360–372. https://doi.org/10.1103/PhysRev.73.360

668 De Rocco, A. G. and Hoover, W. G. (1960). On the interaction of colloidal particles. Proceedings of the
669 National Academy of Sciences, 46:1057–1065. https://doi.org/10.1073/pnas.46.8.1057

670 Derjaguin, B. (1940). On the repulsive forces between charged colloid particles and on the theory of
671 slow coagulation and stability of lyophobe sols. Transactions of the Faraday Society, 35:203–2011.
672 https://doi.org/10.1039/TF9403500180

673 Derjaguin, B. and Landau, L. (1941). Theory of the stability of strongly charged lyophobic soils and of
674 the adhesion of strongly charged particles in solutions of electrolytes. Acta Physicochimica URSS,
675 14(6):633–662. https://doi.org/10.1016/0079-6816(93)90013-L

676 Ebrahimi, D., Whittle, A., and Pellenq, R. (2014). Mesoscale properties of clay aggregates from
677 potential of mean force representation of interactions between nanoplatelets. The Journal of Chemical
678 Physics, 140. https://doi.org/10.1063/1.4870932

679 Ebrahimi, D., Pellenq, R.J.M., Whittle, A.J., 2016. Mesoscale simulation of clay aggregate formation
680 and mechanical properties. Granul. Matter 18, 1–8. https://doi.org/10.1063/1.5011817

681 Everaers, R. and Ejtehadi, M. R. (2003). Interaction potentials for soft and hard ellipsoids. Physical
682 Review E - Statistical Physics, Plasmas, Fluids, and Related Interdisciplinary Topics, 67(4):1–8.
683 https://doi.org/10.1103/PhysRevE.67.041710

684 Gay, J. G. and Berne, B. J. (1981). Modification of the overlap potential to mimic a linear site-site
685 potential. The Journal of Chemical Physics, 74(6):3316–3319. https://doi.org/10.1063/1.441483

686 Gray, C. G. and Stiles, P. J. (2018). Non-linear electrostatics: The poisson-boltzmann equation.
687 European Journal of Physics, 39(5):1–71. https://doi.org/10.48550/arXiv.1803.02507

688 Gupta, A., Govind Rajan, A., Carter, E. A., and Stone, H. A. (2020). Thermodynamics of electrical
689 double layers with electrostatic correlations. Journal of Physical Chemistry C, 124(49):26830–26842.
690 https://doi.org/10.1021/acs.jpcc.0c08554

691 Gupta, V. and Miller, J. D. (2010). Surface force measurements at the basal planes of ordered kaolinite
692 particles. Journal of Colloid And Interface Science, 344(2):362–371.
693 https://doi.org/10.1016/j.jcis.2010.01.012

694 Honório, T., Brochard, L., and Vandamme, M. (2018). Hydration phase diagram of clay particles from
695 molecular simulations. Langmuir, 2017, 33(44):12766–12776.
696 https://doi.org/10.1021/acs.langmuir.7b03198

697 Israelachvili, J. N. (2011). Intermolecular and Surface Forces. Elsevier.

698 Jaradat, K. A. and Abdelaziz, S. L. (2019). Computers and geotechnics on the use of discrete element
699 method for multi-scale assessment of clay behavior. Computers and Geotechnics, 112:329–341.
700 https://doi.org/10.1016/j.compgeo.2019.05.001

701 Kutter, S., Hansen, J. P., Sprik, M., and Boek, E. (2000). Structure and phase behavior of a model clay
702 dispersion: A molecular-dynamics investigation. Journal of Chemical Physics, 112(1):311–322.
703 https://doi.org/10.1063/1.480582

704 Lennard-Jones, J. E. (1931). Cohesion. Proceedings of the Physical Society, 43(5):461–482.
705 https://doi.org/10.1088/0959-5309/43/5/301

706 Liu, J., Lin, C.-L., and Miller, J. D. (2015). Simulation of cluster formation from kaolinite suspensions.
707 International Journal of Mineral Processing, 145:38–47. https://doi.org/10.1016/j.minpro.2015.07.004

708 London, F. (1936). The general theory of molecular forces. Trans. Fara. Soc., 8(8):8–26.
709 https://doi.org/10.1039/TF937330008B

710 Mie, G. (1903). Zur kinetischen Theorie der einatomigen Körper. Annalen der Physik. 316 (8): 657–
711 697. https://doi.org/10.1002/andp.19033160802

712 Mitchell, J. and Soga, K. (2005). Fundamentals of Soil Behavior, 3rd Edition. John Wiley & Sons.

713 Odriozola, G., Romero-Bastida, M., and De, F. (2004). Brownian dynamics simulations of laponite
714 colloid suspensions. Physical Review E - Statistical Physics, Plasmas, Fluids, and Related
715 Interdisciplinary Topics, 70(2):1–15. https://doi.org/10.1103/PhysRevE.70.021405

716 Parsegian, A. V. (2006). Van der Waals forces: A handbook for biologists, chemists, engineers, and
717 physicists. Cambridge University Press. https://doi.org/10.1017/CBO9780511614606

718 Pedrotti, M. and Tarantino, A. (2018). A conceptual constitutive model unifying slurried (saturated),
719 compacted (unsaturated) and dry states. Géotechnique, 69(3):217–233.
720 https://doi.org/10.1680/jgeot.17.P.133

721 Sjoblom, K. (2015). Coarse-grained molecular dynamics approach to simulating clay behavior. Journal
722 of Geotechnical and Geoenvironmental Engineering, 142:06015013.
723 https://doi.org/10.1061/(ASCE)GT.1943-5606.0001394

724 Sridharan, A. and Rao, G. (1973). Mechanism controlling volume change of saturated clays and the role
725 of the effective stress concept. Géotechnique, 23:359–382. https://doi.org/10.1680/geot.1973.23.3.359

726 Thompson, A. P., Aktulga, H. M., Berger, R., Bolintineanu, D. S., Brown, W. M., Crozier, P. S., in 't
727 Veld, P. J., Kohlmeyer, A., Moore, S. G., Nguyen, T. D., Shan, R., Stevens, M. J., Tranchida, J., Trott,
728 C., Plimpton, S. J. (2022). LAMMPS - a flexible simulation tool for particle-based materials modeling
729 at the atomic, meso, and continuum scales. Comp Phys Comm, 271: 10817.
730 https://doi.org/10.1016/j.cpc.2021.108171

731 Verwey, E. J. W. and Overbeek, J. (1948). Theory of the Stability of Lyophobic Colloids: The
732 Interaction of Sol Particles Having an Electric Double Layer. Elsevier, Amsterdam.
733 https://doi.org/10.1038/162315b0

734 Yao, M. and Anandarajah, A. (2003). Three-dimensional discrete element method of analysis of clays.
735 Journal of Engineering Mechanics, pages 585–596. https://doi.org/10.1061/(ASCE)0733-
736 9399(2003)129:6(585)